Epigenetic signatures of regional tau pathology and cognition in the aging and pathological brain.

Short Title: Epigenetic signatures of AD and PART

David C. Goldberg[1,X], Anil R. Wadhwani[2,X], Nadia Dehghani[2], Lasya P. Sreepada[2,3], Hongxiang Fu[1], Philip L. De Jager[4], David A. Bennett[5], David A. Wolk[2], Edward B. Lee[6], PART Working Group, Kurt Farrell[7], John F. Crary[7], Wanding Zhou[1,6]*, Corey T. McMillan[2]*

[1] Center for Computational Genomic Medicine, Children's Hospital of Philadelphia, Philadelphia, PA, USA

[2] Department of Neurology, University of Pennsylvania Perelman School of Medicine, Philadelphia, PA, USA

[3] Department of Bioengineering, University of Pennsylvania School of Engineering and Applied Sciences, Philadelphia, PA

[4] Department of Neurology, Columbia University Irving Medical Center, New York, NY, USA

[5] Rush Alzheimer's Disease Center, Rush University Medical Center, Chicago, IL, USA

[6] Department of Pathology & Laboratory Medicine, University of Pennsylvania Perelman School of Medicine, Philadelphia, PA, USA

[7] Department of Pathology, Department of Artificial Intelligence & Human Health, NASH Family Department of Neuroscience, Ronald M. Loeb Center for Alzheimer's Disease, Friedman Brain Institute, and Neuropathology Brain Bank & Research CoRE, Icahn School of Medicine at Mount Sinai, New York, NY, USA

[X] Equal Contribution

*Co-Corresponding Authors

Corey T. McMillan

Penn Frontotemporal Degeneration Center

3700 Hamilton Walk, Richards 606B

Philadelphia, PA. 19104

(e) mcmillac@pennmedicine.upenn.edu (p) 215 614 0987

&

Wanding Zhou

Center for Computational & Genomic Medicine

Children's Hospital of Philadelphia

3501 Civic Center Blvd

Philadelphia, PA, 19104

(e) wanding.zhou@pennmedicine.upenn.edu (p) 215 5900473

Keywords: epigenetics, aging, tau, Alzheimer's disease, primary age-related tauopathy, DNA methylation

ABSTRACT

Primary age-related tauopathy (PART) and Alzheimer's disease (AD) share hippocampal phospho-tau (p-tau) pathology but differ in p-tau extent and ß-amyloid presence. As a result, PART uniquely enables investigation of amyloid-independent p-tau mechanisms during brain aging. We conducted an epigenome-wide association (EWAS) study of PART, nominating 13 new and robust p-tau/methylation associations. We then jointly analyzed PART and AD epigenomes to develop novel epigenetic clocks, "TauAge", that predict p-tau severity in region-specific, age-, and ß-amyloid-independent manners. Integrative transcriptomic analyses revealed that genes involved in synaptic transmission are related to hippocampal p-tau severity in both PART and AD, while neuroinflammatory genes are related to frontal cortex p-tau severity in AD only. Further, a machine learning classifier trained on PART-vs-AD epigenetic differences stratifies an independent cohort of neuropathologically indeterminate cases into pathological subgroups with disparity in cognitive impairment. Together, these findings demonstrate the brain epigenome's substantial role in linking tau pathology to cognitive outcomes in aging and AD.

Neurofibrillary tangles (NFTs) consisting of hyperphosphorylated tau (p-tau) are a ubiquitous feature of aging present in nearly every human brain older than 50 years of age[1-5]. However, the spatial distribution and within-region severity of p-tau, as well as the associated degree of cognitive impairment, vary widely across individuals, even after accounting for age and co-pathology[6,7]. This is evident in two related conditions, Alzheimer's disease (AD) and Primary Age-Related Tauopathy (PART). In AD, in addition to the accumulation of ß-amyloid-associated neuritic plaques, p-tau originates temporo-limbically before spreading to neocortex[2,8]. In contrast, PART shows p-tau confined to limbic structures in the absence of ß-amyloid plaques[6,9-13]. Therefore, PART and AD are ends of a pathological spectrum that can model p-tau severity and spread in aging.

Apart from their differences, PART and AD share numerous characteristics that have led to the conjecture that PART represents an AD prodrome. P-tau is molecularly similar in PART and AD[6], and there are overlapping genetic variants relating AD risk and Braak NFT stage in PART[14]. However, there are genetic differences between the two conditions as well. We previously identified that a novel locus in the *JADE1* gene as a unique risk determinant of Braak NFT stage in PART[15]. Moreover, as PART progresses, there is increased involvement of the CA2 hippocampal subfield which is largely spared in AD[16]. These findings raise the possibility that inter-individual variation in p-tau severity in PART represents an aging-associated process that is distinct from ß-amyloid associated p-tau pathology in AD[17,18].

Given that DNA methylation (DNAm) changes widely across the lifespan, the epigenome provides an important window into age-associated modifiers of the PART-vs-AD spectrum. While DNAm patterns have been characterized in AD[19-24], prior studies have been limited in several ways. First, blood-derived DNAm epigenetic clocks have linked accelerated epigenetic aging to AD severity[25,26], but the biological basis of these clocks remain obscure and lack brain-specific associations[27]. Second, while studies of cortical brain DNAm have identified CpGs associated with AD neuropathologic change, such as Braak stage NFT distribution[20] and senile plaques[19], they have been performed without regard to within-region severity or the complex interaction of p-tau and ß-amyloid. Therefore, it remains unclear whether these epigenetic changes are a feature of normal brain aging or if they are a consequence of AD pathophysiology.

Here, we hypothesized that an epigenetic program drives variation in hippocampal p-tau pathology in PART. To understand the epigenetic contributions to p-tau in the aging brain we use several computational

approaches to analyze frontal cortex DNAm to disentangle associations between p-tau, ß-amyloid, and aging across the pathological spectrum of PART and AD. This includes the first epigenome-wide association (EWAS) study of PART; the generation of a novel p-tau clock, "TauAge", that is predictive of age-independent p-tau severity in hippocampus and frontal cortex; and a comparative multivariate classifier of PART and AD that distills the shared biological programs contributing to both conditions from those uniquely protective in PART.

RESULTS

Description of cohorts.

We generated frontal cortex DNA methylation profiles for 260 individuals in the PART working group (PWG) cohort comprised of autopsy-confirmed PART cases (Braak NFT stage I-IV, CERAD = None) with digital histology measures of p-tau (NFT) density in AT8-stained tissue sections of hippocampus and frontal cortex, as previously reported[28]. All PWG samples were interrogated using the Illumina EPIC Human Methylation array for ~850K CpGs (Methods: DNAm data generation). We also performed secondary analyses using dorsolateral prefrontal cortical data available from 707 individuals from the Religious Orders Study and the Rush Memory and Aging Project (ROSMAP) cohort[19], which includes 176 cases with PART. Cohort characteristics are summarized in **Supplemental Table 1**. All ROSMAP samples were interrogated for DNAm using the Illumina Human Methylation 450 beadchip array and a subset had matched gene expression data generated by the Illumina TruSeq method with modifications as previously described[29]. The unsupervised clustering of DNA methylomes for each cohort was primarily driven by sex and sample plate and did not reveal relationships to hippocampal p-tau load, Braak stage, or CERAD score (**Extended Data Fig. 1a**). Similarly, DNAm-based cellular deconvolution using a reference atlas of neuronal and glial subtypes yielded largely comparable distributions between the PWG and ROSMAP cohorts, with a slight enrichment of superficial cortical layer cell types in the latter (**Extended Data Fig. 1b-c)**. Nonetheless, cell-type proportion principal components and individual cell-type proportions did not associate with hippocampal p-tau burden in either cohort (**Extended Data Fig. 1d-e**).

An EWAS and a novel epigenetic clock, "TauAge", captures hippocampal tau variation in PART.

To identify biological processes contributing to inter-individual variation in hippocampal p-tau pathology, we performed an EWAS in the PWG cohort (N=260 PART), adjusting for age, sex, and sample plate**.** We identified thirteen CpG sites associated with hippocampal p-tau (FDR < .05), two of which (*cg04905912, cg17649772*) also exceeded the Bonferroni-corrected significance threshold (**Fig. 1a)**. Methylations of these CpGs were positively correlated with one another (**Extended Data Fig. 2a**), suggesting they may be downstream of a common effector or that they may operate in tandem as part of a concerted epigenetic program. To our knowledge, methylation variation at these 13 loci has not been previously associated with tau pathology in aging or AD in prior brain methylation studies[19-24].

Given that DNAm often regulates local gene expression programs[30], we directly evaluated correlations between each of the 13 significant CpGs with RNA-Seq gene expression data of all annotated genes within 10kB of the CpG probe using paired DNAm:RNA-Seq data set from the ROSMAP cohort[29] (Methods: PART Epigenome Wide Association Study). From the 13 CpGs, we identified three significant CpG:gene associations: *cg03815683*:*CDH8*, *cg04522898*:*R3HDM1*, and *cg19212949*:*PEG3*. Downregulation of *CDH8* and *R3HDM1*, but not *PEG3*, further correlated with hippocampal p-tau (**Fig. 1b**). One additional pair (cg03595123:*RTN3*) also had a significant association of gene expression with both CpG methylation and hippocampal p-tau but did not survive FDR<0.05. Thus, p-tau-associated methylation at these newly identified loci correlates with the expression of genes that, in turn, are associated with p-tau pathology in an independent data set.

CpG methylation can also have *trans*-regulatory effects on gene expression[31] so we expanded our analyses to test the correlation of all genes with methylation of the loci identified in our EWAS (Methods: Differential gene expression analysis). We identified a total of 198 genes correlated with CpG methylation , and they were enriched in ontology terms related to ion transport, synaptic transmission, and neuron architecture (**Extended Data Fig. 2b**). Most significant CpG:gene pairs involved *cg04522898* (**Fig. 1c**)*,* suggesting that methylation at this locus may impact large downstream transcriptional networks related to synaptic biology. Together, these findings suggest that p-tau aggregation in the hippocampus is associated with changes in frontal cortical network properties in PART, even in the absence of cortical ß-amyloid deposition.

To further investigate the epigenetic correlates of p-tau pathology in the PWG cohort, we trained a penalized elastic net (EN) regression model, or "clock", to predict age-adjusted hippocampal p-tau residuals (Methods). The resultant hippocampal clock model, "TauAge", consists of 223 CpGs, including *cg18762422* identified by our EWAS. Our model learned the training data with near certainty and closely predicted hippocampal p-tau residuals in testing data (**Fig. 1d**). As expected, given prior adjustments for age, none of these identified CpGs correlated with chronological age (**Extended Data Fig. 2c**). Notably, in contrast to TauAge, existing epigenetic clocks including pan-tissue Horvath[32,33] or brain-specific Cortical[26] clocks were not predictive of age-adjusted residual or unadjusted hippocampal p-tau (**Extended Data Fig. 2d**). These results demonstrate that our novel cortical DNAm clock contains robust signatures indicative of hippocampal p-tau pathological burden in PART, which are separate from known age-related epimutational processes[34].

Distinct TauAge clocks capture p-tau variation in AD cortex and hippocampus

Given the precise predictions using this approach, we next sought to determine if we could accurately calculate TauAge in cases with both p-tau and ß-amyloid pathologies. In AD, NFTs develop earliest in the entorhinal cortex and hippocampus before spreading to the frontal cortex[8]. As a result, NFT burden in the hippocampus and midfrontal cortex are separate but related measures of p-tau severity that vary between individuals. We leveraged the ROSMAP cohort[19], which exhibits a full spectrum of p-tau and ß-amyloid pathologies ranging from PART to AD, to train TauAge models for each region. As before, frontal cortical DNA methylomes were used to predict age-residualized p-tau burden in hippocampus and midfrontal cortex. We observed highly accurate predictions for hippocampal-TauAge (model size: 461 CpGs) and midfrontal-TauAge (model size: 467 CpGs; **Fig. 2a**). Similar to the results in the PWG cohort, the extant cortical and Horvath epigenetic clocks did not accurately predict the p-tau residuals (**Extended Data Fig. 3a**). Neither TauAge model was enriched in aging-associated CpGs within the ROSMAP cohort (**Extended Data Fig. 3b**).

We observed only 8 overlapping CpGs between the hippocampal- and midfrontal-TauAge models. Indeed, while these TauAge models are moderately correlated (**Extended Data Fig. 3c**), hippocampal-TauAge CpGs are less accurate at predicting midfrontal p-tau burden, and similarly midfrontal-TauAge is less accurate at predicting hippocampus p-tau burden (**Fig. 2b**). This regional dissociation suggests that there are regionally-distinct epigenetic signatures that account for variation in p-tau burden. Thus, TauAge does not measure a global

property of the brain but rather reflects separate biologies that contribute to similar pathology in different brain regions.

To account for ß-amyloid-dependent processes that may exacerbate p-tau pathology or confound p-tau-specific epigenetic signatures, we re-trained hippocampal- and midfrontal-TauAge models that, in addition to age, also adjust for total neuritic plaque load (Methods: TauAge model development). The ß-amyloid-adjusted models are also accurate at predicting p-tau burden in respective regions (**Extended Data Fig. 3d)**, have comparable performance to models that only adjust for age, and have substantial overlap in constituent feature CpGs in a region-specific fashion (**Fig. 2c, Supplemental Table 2**). Taken together, this suggests that TauAge CpGs represent an ß-amyloid-independent and regionally-specific epigenetic program.

Hippocampal-TauAge relates to synaptic signaling in PART and AD, whereas midfrontal-TauAge relates to inflammation in AD only.

To disentangle the variable epigenetic loci contributing to each of the TauAge models from PWG and ROSMAP cohorts across regions, we again leveraged paired DNAm:RNA-Seq data from ROSMAP to identify CpG:Gene pairs with each TauAge model (Methods: Differential gene expression analyses). The hippocampal-TauAge gene set was largely distinct from the midfrontal-TauAge gene set, mirroring the regional CpG features selected (**Fig. 2d**, **Extended Data Fig. 3e,** and **Supplemental Table 3**). Strikingly, despite differences in histopathological and DNAm techniques across PWG and ROSMAP cohorts, a highly overlapping gene profile emerged among hippocampal-TauAge models trained separately on PART cases from the PWG cohort, PART cases from the ROSMAP cohort, or all cases from the ROSMAP cohort. The gene ontological profile related to all hippocampal-TauAge models was enriched for synaptic transmission, axon biology, and oxidative phosphorylation terms (**Fig. 2e**), suggesting that hippocampal p-tau accumulation in AD and PART appears to be driven by similar epigenetic and transcriptomic features.

In contrast, consistent with spread of p-tau to frontal cortex that occurs primarily in AD, the CpG:Gene correlations for midfrontal-TauAge were enriched for inflammatory signaling and cytokine production terms. We regressed the expression of the synaptic transmission and inflammation-related genes on regional p-tau and found altered expression of two genes related to synaptic transmission, and five genes related to inflammation

after FDR correction (**Extended Data Fig. 3f)**. Interestingly, one gene, *kinesin family member 5B* **(***KIF5B)*, was common to both midfrontal and hippocampal analyses. Together, these data suggest that hippocampal p-tau severity is associated with altered cortical synaptic activity and connectivity in an ß-amyloid-independent manner both in PART and in AD, while midfrontal p-tau severity may be precipitated by increased inflammation in the cortex in only AD.

Frontal cortex methylations distinguish PART from early AD.

Our TauAge models revealed two epigenomic signatures, one common to PART and AD, and one unique to AD alone. Thus, these observations do not resolve the controversy regarding whether PART simply represents an early pathological prodrome of AD that would eventually manifest with cortical p-tau and ß-amyloid[35] or whether PART represents a distinct neuropathological entity[6]. In an effort to address this controversy, we evaluated whether an epigenetic classification model could be trained to discern subtle PART or AD propensities. To accomplish this, we first compared TauAge in cases at the extremes of the PART-AD neuropathologic spectrum. Additionally, we evaluated the remaining "Indeterminate" cases that fall ambiguously between probable PART and lesser degrees of AD neuropathologic change (CERAD = Sparse, and Braak NFT Stage 0-VI; CERAD = Moderate, and Braak NFT Stage 0-VI; or CERAD = Frequent). Cases with "No Pathology" (CERAD = "None", Braak NFT Stage = 0) were excluded due to their limited number.

As expected, given the pervasive involvement of hippocampus in both diseases, hippocampal-TauAge was greater in AD compared to both PART and Indeterminate cases (**Extended Data Fig. 4a**) and was not distinguishable between PART and Indeterminate cases. In contrast, midfrontal-TauAge showed a progressive increase along the PART-AD continuum, suggesting a direct relationship between inflammation and AD neuropathologic change. Despite significant mean differences, the pathology groups had substantial overlap in TauAge which limited our ability to discriminate pathology using these methylation models alone.

We hypothesized that Indeterminate cases may reflect a heterogeneous group in which a subset of cases are epigenetically more similar to PART while others are more similar to AD. To investigate this possibility, we developed a classifier ("PART-AD classifier") to directly stratify Indeterminate cases as Predicted-PART or Predicted-AD from frontal cortical DNAm (Methods: PART-AD Classifier).

We first trained the PART-AD classifier on a random sample of 80% of PART and AD cases from the ROSMAP cohort, and the model predicted PART vs. AD with 74% accuracy (P=.02) on the remaining 20% of PART and AD cases not seen during feature selection or model training (**Extended Data Fig. 4b-c**). Having validated the approach, we retrained a final model using all PART and AD cases and applied it to cortical DNAm data from 142 individuals defined as Controls (Braak NFT stage 0-II) or AD (Braak NFT stage III-VI) in an external cohort maintained by the Mt. Sinai Brain Bank (**Extended Data Fig. 4d**). The majority of AD cases were classified as Predicted-AD (84%), and the majority of Controls were classified as Predicted-PART (52%). We observed a substantial increase in the percentage of predicted AD cases with increasing Braak NFT stage (**Extended Data Fig. 4e**), thus validating the classifier's performance and the reproducibility of its underlying epigenetic AD signature.

We then applied the PART-AD classifier to stratify indeterminate cases from the ROSMAP cohort as Predicted-AD or Predicted-PART (**Fig. 3a**). Predicted-AD and Predicted-PART cases could not be distinguished clearly from each other directly by their p-tau or neurtitic plaque burden (**Fig. 3b**). Moreover, our TauAge models could not resolve Predicted-AD and Predicted-PART cases (**Extended Data Fig. 4f**), suggesting that the PART-AD classifier measures an orthogonal epigenetic signature.

To further interrogate this additional epigenetic signature, we identified differential methylation at 570 of the classifier feature CpGs (**Fig. 3c, Supplemental Table 4**) in Indeterminate cases that were classified as Predicted-AD or Predicted-PART. Thus, cases of indeterminate pathologic change that do not yet differ substantially in their p-tau burden may have different epigenomes resembling either PART or AD.

Further, we directly compared gene expression of the Predicted-PART and the Predicted-AD cases (Methods: Differential gene expression analyses). Of 4,668 candidate genes, we focused on a subset of 2,179 that were also differentially expressed between confirmed PART and AD and correlated with methylation of any of the 570 CpGs that differed between prediction groups. (**Fig. 3d, Supplemental Table 5**). These Predicted-PART vs. Predicted AD DEGs had highly concordant effect sizes with effect sizes obtained from the confirmed PART vs. AD analysis (**Extended Data Fig. 5a**). Genes upregulated in Predicted-AD compared to Predicted-PART were mildly enriched in processes of cellular migration and development (**Extended Data Fig. 5b**). Moreover, genes upregulated in Predicted-PART compared to Predicted-AD were highly enriched in oxidative

phosphorylation and cellular respiration (**Extended Data Fig. 5c**). This may suggest that the cortical spread of p-tau pathology is preceded by, or may require, cellular metabolic dysfunction. In summary, the PART-AD classifier uses cortical methylation to resolve Indeterminate cases into higher-risk/AD-like and lower-risk/PART-like subgroups with distinct transcriptomic profiles.

Methylation models complement in predicting cognitive impairment.

P-tau pathology is tightly correlated with both age-related and AD-related cognitive impairment[4,36-39]. We, therefore, assessed whether methylation signatures measured by TauAge and the PART-AD classifier were related to cognitive impairment in the ROSMAP cohort, measured by mini-mental status examination (MMSE) ante-mortem median of 1.14 (interquartile range: 0.56 - 4.25) years from brain donation. Both hippocampal and midfrontal-TauAge were inversely correlated with performance on the MMSE (**Fig. 4a**). Interestingly, hippocampal-TauAge could distinguish individuals with mild cognitive impairment (MCI; MMSE 21-23) from those with no cognitive impairment (MMSE ≥ 24) but not from those with dementia-level impairment (MMSE ≤ 20), whereas a prior epigenetic clock could not[25]. On the other hand, midfrontal-TauAge differentiated MCI from individuals with dementia, but not from those who have less cognitive impairment. Together, the two TauAge models can separate individuals along the spectrum of cognitive impairment, likely reflecting their close association with underlying regional p-tau severity.

Despite similarities in p-tau burden in prediction groups identified by the PART-AD classifier, Predicted-PART individuals scored higher on the MMSE than Predicted-AD individuals (**Fig. 4b**). Interestingly, the effect of hippocampal-TauAge on MMSE is more pronounced in the Predicted-AD individuals than in Predicted-PART individuals (**Fig. 4c**). Therefore, while PART and AD share similar hippocampal p-tau, susceptibility to metabolic dysfunction and immune cell infiltration may result in more dramatic cognitive impairment in AD. As a corollary, PART resistance to metabolic dysfunction and lack of inflammation may mediate more resilient cognitive aging.

Finally, to quantify the relative contributions of the TauAge and the PART-AD classifier signatures in predicting cognitive resilience, we constructed several multiple regression models and evaluated the variance explained in MMSE (**Fig. 4d**). While age alone explained only 6.4% of the overall variance in MMSE performance, adding the methylation-based models above increased the adjusted R-squared to 28.3%.

Hippocampal-TauAge, midfrontal-TauAge, and the PART-AD classifier additively improved the summative model's performance, suggesting that each may measure a distinct aspect of pathophysiology that contributes to cognitive impairment in aging and AD.

DISCUSSION

This study establishes an epigenetic landscape of PART. By carefully disentangling correlations between p-tau, ß-amyloid, and DNAm, across a neuropathological spectrum of PART and AD we define an ß-amyloid-independent epigenetic clock linked with regional p-tau pathology. Two key processes – synaptic signaling and neuroinflammation – differentially associate with early hippocampal p-tau and its later spread to the frontal cortex, respectively. Critically, these findings highlight important molecular insights into age- and AD-associated p-tau biology, discussed below in detail.

TauAge is a novel methylation-based measure of within-region p-tau severity.

TauAge predicted hippocampal p-tau variation in PART with high accuracy, outperforming existing epigenetic clocks. TauAge has several key properties that distinguish it from more nonspecific measures of epigenetic aging. First, TauAge reflects brain-specific biological processes that are age-independent. Second, TauAge focuses on within-region severity in p-tau burden whereas prior studies focused on DNAm associations with Braak NFT stage, a measure of the anatomic extent of p-tau spread. Third, the TauAge approach results in region-specific clocks, whereas most epigenetic models aggregate different tissues and pathologies, attributing them to a single age-related biological process. Critically, this is the first demonstration that subsets of cortical DNAm loci can differ with regards to local and remote pathology, and that both can be measured simultaneously.

We replicated our approach in an independent cohort, both when constrained to only PART individuals and when including the full spectrum of AD neuropathologic change. Given these findings, TauAge may be a useful tool to further interrogate the underlying biology of p-tau aggregation and spread. Additional studies that similarly combine DNAm with careful quantitative histopathology are needed to evaluate the generalizability of the TauAge approach, and such studies have the potential to better elucidate region specific age- or pathology-related brain changes.

A key difference between PART and AD is the relative sparing of p-tau inclusions in the frontal cortex in PART. Midfrontal-TauAge and our PART-AD classifier could distinguish individuals with dementia from those with mild cognitive impairment, likely leveraging an AD-specific epigenetic signature related to a T-cell and macrophage-mediated axis of inflammation. Our findings from the PART-AD classifier and the midfrontal-TauAge model add to the growing evidence that PART and AD may have distinct molecular bases. Based on the current observations and our prior genetic studies[14,15], we posit that PART may reflect a model of resistance to p-tau spread that is moderated through both epigenetic and genetic factors.

DNAm can be associated with hippocampal p-tau pathology in aging independently of ß-amyloid.

We identified 13 novel CpGs and nominated three candidate genes (*CDH8*, *R3HDM1*, and *PEG3*) as potential *cis* mediators of tau-associated DNAm. These genes have been linked to altered neuronal connectivity[40-43]. For instance, the *R3HDM1* gene has been linked with age with DNAm at *cg04522898* in whole blood.[44] The *R3HDM1* locus harbors the *pri-miR-128-1* gene[45], and miR-128 has been implicated in synaptic plasticity and cellular survival by additional epigenetic mechanisms[46-48]. Indeed, when we expanded our study to assess for additional CpG-gene expression relationships, we found 198 genes that were differentially expressed in relation to differential methylation of at least one of the 13 CpG sites. A majority of these transgene expression effects, including on *MAPT*, were related to methylation at *cg04522898* which lies within the *R3HDM1* locus and may relate to miR-128 function. While functional validation is required to directly investigate the potential mechanistic role of these genes in tau biology, this study points to several novel genomic loci that may contribute mechanistically to p-tau aggregation in hippocampus.

Synaptic signaling is a shared determinant of hippocampal p-tau burden in both PART and AD.

Synapse dysfunction is a key early hallmark of AD[47,48]. Similarly, synaptic dysregulation may occur in aging and in PART, though there is less consensus on specific molecular etiologies[49-53]. In this study, we demonstrate strong associations between p-tau pathology and synaptic transmission genes. Interestingly, we also find that increased expression of *kinesin family member 5B* (*KIF5B)*, a microtubule motor associated with lysosomal function and mitochondrial localization, positively correlates with hippocampal and midfrontal p-tau[59,60]. This

observation converges with a similar observation in the P301S murine model of tauopathy[61]. Therefore, abnormal cytoskeletal trafficking may synergistically connect to abnormal tau pathology.

Our findings independently corroborate but are unique from prior transcriptomic studies in AD brain, that similarly implicate synaptic dysregulation in AD[62-65]. We first identify DNAm differences associated with hippocampal p-tau and then relate differential methylation to differential gene expression. Moreover, in our study, we focused on the subset of CpGs and associated genes that are likely to be ß-amyloid-independent p-tau modifiers. Lastly, ours is the only study to specifically analyze individuals with PART, and we find that differential methylation converged on overlapping synapse-related genes in both the PWG and ROSMAP cohorts.

PART represents a cognitively resilient form of aging.

Our machine learning-based analyses of DNAm suggest that AD and PART both involve dysregulation of synaptic transmission and plasticity, raising the possibility that PART can set the stage for the development of AD. Individuals with lower p-tau burden than expected for their age exhibit an epigenetic signature indicative of preserved synaptic function, which may confer protection against the onset of ß-amyloid aggregation. In other words, we suspect that a component of the age-associated AD risk is due to underlying PART. Further research is required to determine whether ß-amyloid-independent brain DNA methylation differences consistently predict susceptibility to hippocampal p-tau pathology in additional datasets.

Importantly, our PART-AD classifier uses an epigenetic signature distinct from the TauAge models to stratify cases with indeterminate pathology. Gene ontology analysis identified a role for increased metabolic capacity in Predicted-PART cases and increased cell migration and transcription in Predicted-AD. Given numerous other reports of inflammation-associated transcriptomic changes in brain[66-70], the latter may represent an effect of infiltrating inflammatory cells, and this can be evaluated in more detailed studies using single-cell RNA sequencing or spatial transcriptomics.

Both p-tau and neuritic plaque burden were similar in Predicted-PART and Predicted-AD cases. Strikingly, those predicted as PART exhibited better cognitive performance. Within Predicted-PART cases, there was still an appreciable decline in cognitive performance associated with higher TauAge; however, this effect was far

more pronounced in Predicted-AD cases. This suggests a potential additive effect of synaptic dysregulation and inflammation on cognition in AD.

Importantly, our three novel methylation models relate to distinct underlying biology and synergistically measure cognitive impairment, as evidenced by the increased variance explained in MMSE performance with a summative model that includes all three methylation models. Hippocampal-TauAge can distinguish MCI from the cognitively unimpaired, and it appears to model synaptic pathophysiology shared by PART and AD. Together, these findings lend credence to the hypothesis that age-associated cognitive impairment due to hippocampal dysfunction may precede and be requisite for typical AD.

From here, despite similarities in pathological burden, individuals with early AD begin to diverge from PART in a manner detectable by our PART-AD classifier and related to an epigenetic signature of brain metabolic failure. Finally, as p-tau disseminates widely through the neocortex, midfrontal-TauAge increases, distinguishing MCI from dementia-level of impairment and relating to T-cell-mediated inflammation. This absence of an inflammatory signature in PART cases is potentially neuroprotective and indicates a new pathophysiological axis differentiating PART from AD.

Caveats to Consider and Overall Conclusions

Critically, while unable to directly cross-validate DNAm models across PWG and ROSMAP cohorts, there was substantial intersection of the differentially expressed genes regulated by the respective feature CpGs of the two cohort models of PART. This is notable given the methodological differences across PWG and ROSMAP cohorts. First, the two studies ascertain DNAm using two similar but distinct array chips, which include nonoverlapping sets of CpG sites. Therefore, a model trained on one cohort DNAm may not be directly applied to another dataset unless unique CpGs are excluded, in turn reducing the depth of genomic coverage and biological insight. Second, the two studies used different immunohistochemistry methods that vary in their p-tau affinity. Specifically, in ROSMAP, NFTs were identified by silver stain, which is more sensitive to mature NFTs, whereas in PWG, NFTs were identified by AT8 antibody, which detects both mature and immature p-tau assemblies. Despite these technical differences at the levels of microarray and histopathology, the convergence

of the models at the gene expression level suggests that they are two convergent views of the same underlying biology.

Despite these caveats, our epigenetic models clarify molecular similarities and differences between AD and PART and highlight a role for age-independent interindividual variation in hippocampal p-tau severity as a separate modifiable risk factor for AD and age-associated cognitive changes more broadly.

LEGENDS

Fig. 1: Hippocampal p-tau burden in PART associates with a DNAm signature related to synaptic signaling and cytoskeletal architecture.

- **a)** Epigenome-wide association study (EWAS) of hippocampal p-tau, covarying for age, sex, and batch, reveals 13 novel CpGs (red). Dashed line indicates level of significance after correction for multiple comparisons: False Discovery Rate (FDR) < 0.05 (Black) and Bonferroni-adjusted p-value < 0.05 (Blue).
- **b)** Table of EWAS CpGs and adjacent genes, along with effect size of hippocampal p-tau burden on CpG methylation (blue outline) in PWG cohort, Pearson correlation coefficients of CpG methylation and gene expression (green outline) in ROSMAP cohort, and effect size of hippocampal p-tau burden on gene expression (red outline) in ROSMAP cohort. Not all CpG:gene pairs could be tested in both cohorts due to lack of detectable RNA expression or absence of a CpG probe on the Human Methylation450 (HM450) beadchip array. n = number of cases. kb = kilobase.
- **c)** Compared to other EWAS CpGs, methylation at *cg04522898* correlates with the expression of a large network of genes related to synaptic transmission, neuron projection, and ion transport. Red edges = positive correlation, blue edges = negative correlation.
- **d)** TauAge predicts age-adjusted hippocampal p-tau residuals with high accuracy in the PWG cohort. [Training] n = 174, Pearson's Cor = 0.9997 and P < 2.2e-16; [Testing] n = 86, Cor=0.77 and P < 2.2e-16. F = female, M = male.

Fig. 2: TauAge predicts p-tau severity in a region-specific manner.

- **a)** TauAge predicts both hippocampal (left) and midfrontal (right) age-adjusted p-tau residuals with high accuracy in the ROSMAP cohort. For hippocampal-TauAge, one outlier is not displayed due to axes limits but was included in statistical testing. [hippocampus, training] n = 416, Pearson Cor = 0.9997 and P = 0; [hippocampus, testing] n = 291, Pearson Cor = 0.66, P = 1.342e-37; [midfrontal, training] n = 416, Cor = 0.9996 and P = 0; [midfrontal, testing] n = 291, Pearson Cor = 0.69 and P = 1.68e-42. F = female, M = male.
- **b)** In contrast to TauAge, region-discordant models fail to predict p-tau residuals. Models trained to predict hippocampal age-adjusted p-tau residual from midfrontal p-tau EWAS CpGs (left) do not learn or perform as well as the region-concordant hippocampal-TauAge model. The same is true for the converse condition (right). [hippocampal, training] n = 416, Pearson's Cor = 0.66 and P = 1.19e-54; [hippocampus, testing] n = 291, Pearson's Cor = 0.197 and P = 0.0007; [midfrontal, training] n = 416, Pearson's Cor = 0.64 and P = 8.4e=-49; [midfrontal, testing] n = 291, Pearson's Cor = 0.305 and P = 1.09e-7. F = female, M = male.
- **c)** Upset plot demonstrating number of disparate and overlapping final feature CpGs in each TauAge model. The overlapping CpGs from the unadjusted and amyloid-adjusted TauAge models are suspected to be amyloid-independent epigenetic modifiers of p-tau in hippocampus (purple) and midfrontal cortex (orange).
- **d)** Heatmap demonstrates substantial enrichment of methylation-associated gene expression in hippocampal-TauAge models developed from PART cases in two independent cohorts. This enrichment is shared with the amyloid-adjusted hippocampal-TauAge model from all cases in the ROSMAP cohort, but distinct from the amyloid-adjusted midfrontal-TauAge model genes from the same set of individuals. R = ROSMAP Cohort. P = PWG group cohort. Amyloid-Ind = Genes associated with Amyloid-independent CpG as denoted in Fig 2c.
- **e)** The feature CpGs of each hippocampal-TauAge model are associated with expression of genes enriched for gene ontology (GO) terms related to synaptic transmission, oxidative phosphorylation, and cytoskeletal architecture. In contrast, the feature CpGs of the midfrontal-TauAge model are associated with expression of genes enriched for GO terms related to inflammation. Statistical testing is detailed in Methods.

Fig. 3: The PART-AD classifier measures an additional epigenetic signature that distinguishes PART from AD.

- **a)** Schematic of training and application of the PART-AD classifier. DNAm from cases meeting definition for PART (n=176) or AD (n=118) from the ROSMAP cohort were used to train a support vector machine, which was in turn used to stratify Indeterminate cases (n = 404) from the ROSMAP cohort into Predicted-PART and Predicted-AD cases for subsequent analyses.
- **b)** Hippocampal (Hipp) and midfrontal (MF) p-tau neurofibrillary tangles (NFTs) and midfrontal and total ß-amyloid neuritic plauqes were similar between Predicted-PART and Predicted-AD cases. Pairwise t-tests n = 366. n.s = not significant.
- **c)** Volcano plot of differentially methylated CpGs between Predicted-PART and Predicted-AD cases from the ROSMAP cohort (Model: CpG methylation ~ age + sex + sample_plate + prediction group): n = 366. Highlighted are 570 significant CpGs after correction with an FDR < 0.05 (red line).
- **d)** Analysis of ROSMAP RNA-sequencing data reveals 4,668 differentially expressed genes between Predicted-PART and Predicted-AD. Highlighted in red (upregulated) and blue (downregulated) are 2,179 of these genes that are also associated with differential-methylation at a feature CpG of the PART-AD classifier and were differentially expressed between confirmed PART and AD.

Fig. 4: TauAge and the PART-AD classifier estimate cognitive impairment better than age or neuropathologic change alone.

- **a)** Increasing hippocampal (left) and midfrontal (right) TauAge in the ROSMAP cohort are associated with decreasing performance on the mini-mental status examination (MMSE) and, therefore, increasing cognitive impairment. For hippocampal-TauAge, one outlier is not displayed due to axes limits but was included in statistical testing. Statistical test was a one-way ANOVA followed by Tukey's range test: n = 707.
- **b)** Predicted-AD cases exhibit lower MMSE score and, therefore, greater cognitive impairment compared to Predicted-PART cases in the ROSMAP cohort. Statistical test was a two-tailed *t*-test: n = 366.
- **c)** There is an inverse correlation of hippocampal-TauAge and MMSE score. The slope of the effect is driven by an effect in Predicted-AD cases compared to Predicted-PART cases. For hippocampal-TauAge, one outlier is not displayed due to axes limits but was included in statistical testing. [Predicted-PART] n= 417, Cor = -0.055, and P = 0.258; [Predicted-AD] n= 287, Cor = -0.28, and P = 1.59e-06.
- **d)** Hippocampal-TauAge, midfrontal-TauAge, and the PART-AD classifier better correlate with cognitive impairment compared to either age or AD neuropathologic change (ADNC) alone.

Supplemental Table 1: Individual characteristics for the PART Working Group (PWG) and Religious Orders Study and Memory and Aging Project (ROSMAP) cohorts separated by neuropathological case definitions (Methods).

Supplemental Table 2: TauAge feature CpGs.

Supplemental Table 3: TauAge-associated differentially-expressed genes.

Supplemental Table 4: PART-AD classifier feature CpGs.

Supplemental Table 5: Classifier-associated differentially expressed genes.

Extended Data Fig. S1: Methylation structure.

- **a)** T-distributed stochastic neighbor embedding (t-SNE) clustering of DNAm in both cohorts shows organization of data by sex and sample plate, but not hippocampal p-tau burden, Braak NFT stage, or CERAD score.
- **b)** Cell type proportion estimates for 20 major brain cell types from methylation-based deconvolution in PWG and ROSMAP.
- **c)** Principal component analysis using estimated cell type proportions demonstrates mild differences in cell type composition between two cohorts.
- **d)** Regressing hippocampal p-tau burden on cell type proportion principal components demonstrates that p-tau is not significantly associated with an individual sample's cell type composition in either cohort.
- **e)** Regressing hippocampal p-tau on cell type proportions, covarying for age and sex, did not reveal an association for any cell type in PWG cases. FDR = False Discovery Rate

Extended Data Fig. 2: Characterization of PART EWAS and Hippocampal-TauAge CpGs.

- **a)** Heatmap demonstrates that PWG EWAS CpGs are correlated with one another (Pearson's correlation).
- **b)** EWAS CpG methylation is correlated with expression of genes enriched for gene ontology (GO) terms related to synaptic transmission, ion transport, and cytoskeletal architecture. Statistical testing is detailed in Methods.
- **c)** Volcano plot showing effects sizes of aging on CpG methylation in the PWG cohort. Hippocampal-TauAge feature CpGs are age-independent.
- **d)** Epigenetic age acceleration residuals (horizontal axis) calculated by the Horvath pan-tissue clock or Cortical brain-specific clock do not correlate with the actual hippocampal p-tau burden nor the age-adjusted p-tau residual. Statistical test was Pearson correlation. n = 260.

Extended Data Fig. 3: Characterization of ROSMAP hippocampal and midfrontal-TauAge CpGs.

- **a)** Epigenetic age acceleration (horizontal axis) calculated by the Horvath pan-tissue clock (left) and Cortical brain-specific clock (right) do not correlate with hippocampal age-adjusted p-tau in the ROSMAP cohort. Statistical test was Pearson correlation: n = 707 [Horvath], 707 [Cortical].
- **b)** Volcano plot demonstrating that hippocampal (blue) and midfrontal (red) TauAge feature CpGs are largely age-independent in the ROSMAP cohort.
- **c)** Hippocampal and midfrontal-TauAge are moderately correlated (Pearson's cor = 0.366, P = 1.3e-10. One outlier is not displayed due to axes limits but was included in statistical testing. n = 291 TauAge testing cases.
- **d)** Amyloid-adjusted TauAge predicts both hippocampal (left) and midfrontal (right) age- and ß-amyloid-adjusted p-tau residuals with high accuracy in the ROSMAP cohort. [hippocampus, training] n = 416, Pearson Cor = 0.9992 and P = 0; [hippocampus,testing] n = 291, Pearson Cor = 0.75, P = 5.35e-54; [midfrontal, training] n = 416, Cor = 0.9995 and P = 0; [midfrontal, testing] n = 291, Pearson Cor = 0.69 and P = 5.02e-43. F = female, M = male. For hippocampal-TauAge, one outlier is not displayed due to axes limits but was included in statistical testing.
- **e)** Upset plot demonstrating number of overlapping and distinct genes for different TauAge model CpG sets. Genes were identified for correlation with the model CpGs. "Amyloid-independent" corresponds to the CpG sets from Fig. 2C shared between amyloid and non-amyloid adjusted models. R = ROSMAP, P = PWG. Fig. is truncated to highlight overlap. Complete listing of genes in Supplemental Table 3.
- **f)** Violin plots illustrating the effect size of regional p-tau severity on gene expression for synaptic transmission genes identified from hippocampal-TauAge models (left) and inflammation related genes from TauAge midfrontal models (right). Significant genes (FDR<.05) highlighted. Statistical testing is detailed in Methods.

Extended Data Fig. 4: DNAm distinguishes indeterminate cases along the PART-AD continuum.

- **a)** Hippocampal (left) and midfrontal (right) TauAge increase along the PART-AD continuum. Midfrontal-TauAge more strongly distinguishes indeterminate cases from PART. For hippocampal-TauAge, one outlier is not displayed due to axes limits but was included in statistical testing. n= 290 TauAge test cases.
- **b)** Schematic of training and testing of the preliminary PART-AD classifier. DNAm from ROSMAP cases meeting definition for PART (n=141) or AD (n=95) were used to train a support vector machine, which was tested for accuracy on the remaining PART (n=35) or AD (n=23) cases in the ROSMAP cohort.
- **c)** Confusion matrix demonstrating performance of the preliminary PART-AD classifier on testing cases.
- **d)** Schematic of training and testing of the final PART-AD classifier. DNAm from all ROSMAP cases meeting definition for PART (n=176) or AD (n=118) were used to train a support vector machine, which was then applied to an external cohort from the Mount Sinai Brain Bank (MSBB).
- **e)** Proportion of cases by Braak NFT stage within the MSBB cohort that are classified as Predicted-PART or Predicted-AD by the PART-AD Classifier. Note that in this cohort, cases are defined as AD (Braak NFT stage III-VI) or control (Braak NFT stage 0-II), without regard to ß-amyloid status. Therefore, some cases that meet our definition of PART may be present in both groups.
- **f)** Predicted-AD and Predicted-PART in the ROSMAP cohort cases could not be distinguished by either unadjusted or amyloid-adjusted TauAge models. For hippocampal-TauAge, one outlier is not displayed due to axes limits but was included in statistical testing. Pairwise t-tests: n = 366. n.s. = not significant.

Extended Data Fig. 5: Predicted-PART and Predicted-AD have a distinct transcriptomic signature.

- **a)** Correlation of differential gene expression effect size between PART and AD cases (horizontal axis) and Predicted-PART and Predicted-AD cases (vertical axis) for all highlighted genes in (a) Pearson Cor = 0.97 and $P < 2.2e-16$.
- **b)** Genes upregulated in Predicted-PART compared to Predicted-AD are enriched for gene ontology (GO) terms related to oxidative phosphorylation and cellular respiration. Statistical testing is detailed in Methods.
- **c)** Genes upregulated in Predicted-AD compared to Predicted-PART are enriched for gene ontology (GO) terms related to cell differentiation and migration. Statistical testing is detailed in Methods.

ONLINE METHODS

Patient Selection and Cohorts. Fresh-frozen brain tissue was obtained from the contributing centers in the PART Working Group (PWG) as previously described[15]. Inclusion criteria were individuals with normal cognition, mild cognitive impairment (any type) and dementia. Cognitive status was determined either premortem or postmortem by a clinical chart review, mini-mental score, or clinical dementia rating[71,72]. Neuropathological assessments were performed at the respective centers using standardized criteria including Consortium to Establish a Registry for Alzheimer's Disease (CERAD) neuritic plaque assessment and Braak neurofibrillary tangle staging.[8,73] In addition, formalin fixed paraffin-embedded tissue sections were obtained and reevaluated by the study investigators to confirm the lack of Aβ and degree of PART p-tau pathology as previously described[16]. Clinical exclusion criteria were motor neuron disease, parkinsonism, and frontotemporal dementia. Neuropathological exclusion criteria were other degenerative diseases associated with NFTs (i.e., AD, progressive supranuclear palsy [PSP], corticobasal degeneration [CBD], chronic traumatic encephalopathy [CTE], frontotemporal lobar degeneration-tau [FTLD-tau], Pick disease (PiD), Guam amyotrophic lateral sclerosis/parkinsonism–dementia, subacute sclerosing panencephalitis, globular glial tauopathy). Individuals with aging-related tau astrogliopathy (ARTAG) were not excluded[74]. Characteristics and procedures of the Religious Orders Study and Memory and Aging Project (ROSMAP) were as previously described[75]. Characteristics and procedures of the Mount Sinai Brain Bank (MSBB) cohort were as previously described[76].

Case definitions and histopathology. To allow for comparisons between cohorts and to minimize confounding due to overlapping pathologies, we limited our analyses using the following case definitions, using variables common across PWG and ROSMAP cohorts. We conserve our definition of PART to "definite PART" defined as Braak NFT stage I-IV and CERAD = None[6]. For AD, we restrict to cases that meet Braak NFT stage VI-V and CERAD = Frequent[17]. Remaining cases were termed Indeterminate. Digital histopathology in the PWG cohort was performed as previously described[77]. Briefly, stains were performed on 4 μm-thick formalin-fixed paraffin-embedded (FFPE) sections stained with AT8 antibody. Sections from the body of the hippocampus were targeted, but this neuroanatomical landmark was not represented in all sections, and there was some variability noted with regard to representation along the anterior–posterior axis. Whole slice images were scanned using an Aperio CS2 (Leica Biosystems, Wetzlar Germany) digital slide scanner at 20 × magnification, and neurofibrillary tangle density was calculated via a SegNet model architecture as previously detailed[28]. Manual histopathology assessment in the ROSMAP cohort was performed by independent neuropathological assessment of silver-stained tissue, as previously described[78]. To validate the PART-AD classifier, we tested it on cases from the MSBB cohort, which the investigators previously defined as Control (Braak NFT Stage 0-II), or Late Stage AD (Braak NFT Stave V-VI).

DNAm data generation. In the PWG cohort, DNA was extracted from the frontal cortex. Bisulfite converted DNA was profiled using the Illumina Infinium MethylationEPIC bead chip array at the Center for Applied Genomics core at the Children's Hospital of Philadelphia. In the ROSMAP cohort, DNA extraction and methylation profiling using the Illumina Infinium Human Methylation450 bead chip assay was performed as previously described[19]. Raw data from both cohorts was used and subjected to the same standard manufacture recommended preprocessing and quality control pipeline using the SeSAMe R package (version 1.22.0). Beta values were extracted using the openSesame function with default parameters as previously described[79].

Unsupervised clustering analysis: CpGs with >50% missingness across all samples were removed and remaining missing values were imputed using the beta value mean from non-missing samples. tSNE analysis was performed using the Rtsne package (version 0.16) with a perplexity of 30.

Cell type deconvolution: Beta matrices for PWG and ROSMAP cohorts were filtered for common CpGs with coverage across 75% or more of samples in both cohorts. A reference matrix for 20 major brain cell types was constructed by performing one vs. all non-parametric analyses of pseudobulk methylomes obtained from publicly availably single cell WGBS data[80-82]. Reference-based cellular deconvolution was performed using the EpiDISH R package (version 2.16.0) with the robust partial correlations (RPC) method. Principal component analysis was performed with the prcomp function from the stats package (version 4.4.0) using the cell type proportions as input features.

PART Epigenome Wide Association Study (EWAS): CpG methylation (CpGm) was regressed on logarithmically-transformed hippocampal p-tau (hip_p-tau) with age, sex and sample plate added as covariates. [Model: CpGm ~ age + sex + sample plate + *log*(hip_p-tau + 1)] Modelling was performed using the DML() function from the SeSAMe R package (version 1.22.0). P values for each modelled CpG were corrected for multiple comparisons by the false discovery rate (FDR) method, and only those with FDR < .05 were considered for further analysis. Gene annotations were retrieved using the sesameData_txnToGeneGRanges function from the sesameData package (version 1.21.9) and intersected with EWAS hit CpGs (expanded by 10kb) using the subsetByOverlaps function from the GenomicRanges package (version 1.57.1).

TauAge model development: TauAge is a novel statistical model that uses methylation at a distinct set of feature CpGs to predict an age-adjusted regional p-tau residual. To calculate the age-adjusted p-tau residual, logarithmically-transformed hippocampal or midfrontal p-tau was regressed on age [*log*(p-tau + 1) ~ age]. Amyloid-adjusted TauAge similarly predicts an age- and amyloid-adjusted p-tau residual. To calculate age- and amyloid-adjusted residuals, logarithmically-transformed total brain neuritic plaques were added as a covariate [*log*(p-tau + 1) ~ age + *log*(plaque + 1)]. For each model, training data were balanced to include equal numbers of male and female samples (80% of lesser-represented sex), and remaining samples were used for testing. For any given cohort and region, an elastic net (EN) regression of p-tau residuals on CpGm was performed using the cv.glmnet function from the glmnet package (version 4.1.8) with an alpha parameter of 0.5 and 10-fold cross validation. For each p-tau residual target, CpG features were rank ordered according to the unadjusted P-value from running a univariate EWAS [Model: CpGm ~ age + sex + sample plate + *log*(variable + 1)]. Feature sizes were scanned from the top 2,000- to top 30,000-ranked CpGs, and models with the most highly correlated predictions to actual values on testing data were selected for further analysis. For hippocampal-TauAge, there was one outlier in the ROSMAP cohort was 6 standard deviations below the cohort mean. This outlier was excluded from visualization but was included in all statistical analyses. To confirm the within-region specificity of TauAge models in the ROSMAP cohort, separate models were trained to predict one region's p-tau residual using the opposite region's feature CpGs.

Epigenetic age analysis: Missing values from processed beta matrices were imputed using the row mean from non-missing samples, and epigenetic age estimates (mAge) were computed using the methyAge function from the dnaMethyAge package (version 0.2.0)[83]. Age acceleration was computed by calculating the residual of epigenetic age regressed onto the chronological age [mAge ~ Age]. Pearson correlations were computed between the age acceleration residuals and p-tau load or p-tau residual.

PART-AD classifier development: Initial models were trained on 80% of randomly sampled AD cases (n=95) and 80% of randomly sampled PART cases (n=141). For feature selection, CpG methylation was regressed on pathology group (PART vs. AD) with age, sex and sample plate added as covariates (Model: CpGm ~ age + sex + sample plate + pathology) and the top 1000 CpGs associating with pathology group by P value were selected for model features. PART cases were those with Braak staging I-IV and a CERAD score of None, while AD cases were those with Braak stage V-VI, CERAD score of Frequent. Model performance was evaluated in the held out 20% of cases from each pathology group. For the final model, all PART and AD cases were used with the same feature selection process. Feature selection modelling was performed using the DML function from the SeSAMe R package (version 1.22.0) and support vector machine classifiers trained using the svm function (kernel="linear") from the e1071 package (version 1.7-14). For CpGs with missing values during model training or testing, the mean over all other samples was used for imputation. Performance statistics were computed using the Caret library (version 6.0-94)[84].

Differential gene expression analysis: Fragments per kilobase of transcript per million mapped reads (FPKM)-normalized gene expression data from the ROSMAP cohort was log transformed and tested for correlation with methylation of PART EWAS CpGs, TauAge feature CpGs, or PART-AD Classifier feature CpGs. Correlations were FDR-adjusted and CpG methylation:gene expression pairs with an absolute effect size value >= .2 and FDR < .0001 were filtered for further analysis. Only cases where both DNAm and RNA-sequencing data were available were included. To identify genes differentially expressed between AD:PART or Predicted-AD:Predicted-PART, linear models were fit for each gene using the lmFit function from the Limma R package (3.58.1). The variance of a gene was stabilized using the eBayes function. DEGs were identified with a moderated t-test using the decideTests function with default parameters. To identify genes associated with p-

tau pathology, gene expression for each gene was regressed on log transformed p-tau using the lm() function and genes with an FDR<.05 were considered for further analyses. All gene ontology analyses were performed using Enrichr[85-87].

Statistical testing (Predicted-PART vs. Predicted-AD): Standard two-tailed t-tests were performed using the t.test function (stats 4.4.0) between Predicted-PART and Predicted-AD to compare mean TauAge, NFTs (hippocampal and midfrontal), neuritic plaques (midfrontal, total) and MMSE. Multiple testing was corrected using the FDR method.

Acknowledgements

We wish to thank all the individual study volunteers, tissue donors, and caregivers with whom this work would not be possible. This work was supported by funding from the National Institutes of Health (R01 AG054008, R01 AG060961, R01 AG062348, R01AG066152, P30AG072979, R01 NS095252, R01 NS086736, R35GM146978, K01 AG070326, P01AG066597, P01AG084497, P30 AG066514, T32AG076411, UE5NS065745), CurePSP 685-2023-06-Pathway, the Rainwater Charitable Foundation / Tau Consortium, Karen Strauss Cook Research Scholar Award, and Penn Institute on Aging. The results published here are in whole or in part based on data obtained from the AD Knowledge Portal. Study data were provided by the Rush Alzheimer's Disease Center, Rush University Medical Center, Chicago. Data collection was supported through funding by P30AG10161, P30AG72975, R01AG15819, R01AG17917, R01AG30146, R01AG36836, U01AG46152, U01AG61356, and the Illinois Department of Public Health (ROSMAP). Additional phenotypic data can be requested at www.radc.rush.edu. Brain banking and neuropathology assessments for the MSBB cohort were supported by NIH grants AG02219, AG05138, and MH064673 and the Department of Veterans Affairs VISN3 MIRECC.

Data Availability Statement

The data that support the findings of this study are available on reasonable request from the corresponding author. The data are not publicly available due to privacy or ethical restrictions.

Competing Interests Statement

DCG, ARW, ND, LPS, EBL, DAB, HF, PLD, KF, JFC, WZ, and CTB have no competing interests to declare. DAW has served as a paid consultant to Eli Lilly, GE Healthcare, Beckman Coulter and Qynapse; serves on a DSMB for Functional Neuromodulation and GSK; and was a site investigator for a clinical trial sponsored by Biogen.

Author Contributions

Conceptualization: CTM and WZ. Study design and methodology: DCG, ARW, CTM, and WZ. Collection of data: JFC, KF, DAB, EBL Data Analysis: DCG, ARW, ND. Manuscript writing: ARW, DCG, CTM, and WZ. Manuscript editing: ARW, DCG, ND, LPS, EBL, DAW, DAB, CTM, WZ. Resources and funding: CTM and WZ.

REFERENCES

1 Bouras, C., Hof, P. R. & Morrison, J. H. Neurofibrillary tangle densities in the hippocampal formation in a non-demented population define subgroups of patients with differential early pathologic changes. *Neuroscience letters.* **153**, 131-135 (1993). https://doi.org/10.1016/0304-3940(93)90305-5

2 Braak, H., Thal, D. R., Ghebremedhin, E. & Del Tredici, K. Stages of the Pathologic Process in Alzheimer Disease: Age Categories From 1 to 100 Years. *Journal of Neuropathology & Experimental Neurology* **70**, 960-969 (2011). https://doi.org/10.1097/nen.0b013e318232a379

3 Sonnen, J. A. Ecology of the Aging Human Brain. *Archives of Neurology* **68**, 1049 (2011). https://doi.org/10.1001/archneurol.2011.157

4 Ganz, A. B. *et al.* Neuropathology and cognitive performance in self-reported cognitively healthy centenarians. *Acta Neuropathol Commun* **6**, 64 (2018). https://doi.org/10.1186/s40478-018-0558-5

5 Cholerton, B. *et al.* Neuropathologic Burden and Dementia in Nonagenarians and Centenarians: Comparison of 2 Community-Based Cohorts. *Neurology* **102**, e208060 (2024). https://doi.org/10.1212/WNL.0000000000208060

6 Crary, J. F. *et al.* Primary age-related tauopathy (PART): a common pathology associated with human aging. *Acta Neuropathologica* **128**, 755-766 (2014). https://doi.org/10.1007/s00401-014-1349-0

7 Jefferson-George, K. S., Wolk, D. A., Lee, E. B. & Mcmillan, C. T. Cognitive decline associated with pathological burden in primary age-related tauopathy. *Alzheimer's & Dementia* **13**, 1048-1053 (2017). https://doi.org/10.1016/j.jalz.2017.01.028

8 Braak, H. & Braak, E. Neuropathological stageing of Alzheimer-related changes. *Acta neuropathologica.* **82**, 239-259 (1991). https://doi.org/10.1007/BF00308809

9 Jellinger, K. A. *et al.* PART, a distinct tauopathy, different from classical sporadic Alzheimer disease. *Acta Neuropathologica* **129**, 757-762 (2015). https://doi.org/10.1007/s00401-015-1407-2

10 Wang, X. *et al.* Primary age-related tauopathy in a Chinese cohort. *Journal of Zhejiang University-SCIENCE B* **21**, 256-262 (2020). https://doi.org/10.1631/jzus.b1900262

11 Savola, S. *et al.* Primary age-related tauopathy in a Finnish population-based study of the oldest old (Vantaa 85+). *Neuropathol Appl Neurobiol* **48**, e12788 (2022). https://doi.org/10.1111/nan.12788

12 Nelson, P. T. *et al.* Brains With Medial Temporal Lobe Neurofibrillary Tangles But No Neuritic Amyloid Plaques Are a Diagnostic Dilemma But May Have Pathogenetic Aspects Distinct From Alzheimer Disease. *Journal of Neuropathology & Experimental Neurology* **68**, 774-784 (2009). https://doi.org/10.1097/nen.0b013e3181aacbe9

13 Mungas, D., Tractenberg, R., Schneider, J. A., Crane, P. K. & Bennett, D. A. A 2-process model for neuropathology of Alzheimer's disease. *Neurobiology of Aging* **35**, 301-308 (2014). https://doi.org/10.1016/j.neurobiolaging.2013.08.007

14 Mcmillan, C. T. *et al.* Alzheimer's genetic risk is reduced in primary age-related tauopathy: a potential model of resistance? *Annals of Clinical and Translational Neurology* **5**, 927-934 (2018). https://doi.org/10.1002/acn3.581

15 Farrell, K. *et al.* Genome-wide association study and functional validation implicates JADE1 in tauopathy. *Acta Neuropathologica* **143**, 33-53 (2022). https://doi.org/10.1007/s00401-021-02379-z

16 Walker, J. M. *et al.* Early Selective Vulnerability of the CA2 Hippocampal Subfield in Primary Age-Related Tauopathy. *J Neuropathol Exp Neurol* **80**, 102-111 (2021). https://doi.org/10.1093/jnen/nlaa153

17 Montine, T. J. *et al.* National Institute on Aging–Alzheimer's Association guidelines for the neuropathologic assessment of Alzheimer's disease: a practical approach. *Acta Neuropathologica* **123**, 1-11 (2012). https://doi.org/10.1007/s00401-011-0910-3

18 Crary, J. Primary age-related tauopathy and the amyloid cascade hypothesis: the exception that proves the rule? *Journal of Neurology and Neuromedicine* **1**, 53-57 (2016). https://doi.org/10.29245/2572.942x/2016/6.1059

19 De Jager, P. L. *et al.* Alzheimer's disease: early alterations in brain DNA methylation at ANK1, BIN1, RHBDF2 and other loci. *Nat Neurosci* **17**, 1156-1163 (2014). https://doi.org/10.1038/nn.3786

20 Smith, R. G. *et al.* A meta-analysis of epigenome-wide association studies in Alzheimer's disease highlights novel differentially methylated loci across cortex. *Nature Communications* **12** (2021). https://doi.org/10.1038/s41467-021-23243-4

21 Shireby, G. *et al.* DNA methylation signatures of Alzheimer's disease neuropathology in the cortex are primarily driven by variation in non-neuronal cell-types. *Nature Communications* **13** (2022). https://doi.org/10.1038/s41467-022-33394-7
22 Lang, A.-L. *et al.* Methylation differences in Alzheimer's disease neuropathologic change in the aged human brain. *Acta Neuropathologica Communications* **10** (2022). https://doi.org/10.1186/s40478-022-01470-0
23 Li, Z. *et al.* Differential DNA methylation in the brain as potential mediator of the association between traffic-related PM(2.5) and neuropathology markers of Alzheimer's disease. *Alzheimers Dement* **20**, 2538-2551 (2024). https://doi.org/10.1002/alz.13650
24 Zhang, J. *et al.* Integrative multi‐omics analysis reveals the critical role of the <scp>PBXIP1</scp> gene in Alzheimer's disease. *Aging Cell* (2023). https://doi.org/10.1111/acel.14044
25 Thrush, K. L. *et al.* Aging the brain: multi-region methylation principal component based clock in the context of Alzheimer's disease. *Aging (Albany NY)* **14**, 5641-5668 (2022). https://doi.org/10.18632/aging.204196
26 Shireby, G. L. *et al.* Recalibrating the epigenetic clock: implications for assessing biological age in the human cortex. *Brain* **143**, 3763-3775 (2020). https://doi.org/10.1093/brain/awaa334
27 Bell, C. G. *et al.* DNA methylation aging clocks: challenges and recommendations. *Genome Biology* **20** (2019). https://doi.org/10.1186/s13059-019-1824-y
28 Marx, G. A. *et al.* Artificial intelligence-derived neurofibrillary tangle burden is associated with antemortem cognitive impairment. *Acta Neuropathol Commun* **10**, 157 (2022). https://doi.org/10.1186/s40478-022-01457-x
29 Mostafavi, S. *et al.* A molecular network of the aging human brain provides insights into the pathology and cognitive decline of Alzheimer's disease. *Nature Neuroscience* **21**, 811-819 (2018). https://doi.org/10.1038/s41593-018-0154-9
30 Moore, L. D., Le, T. & Fan, G. DNA Methylation and Its Basic Function. *Neuropsychopharmacology* **38**, 23-38 (2013). https://doi.org/10.1038/npp.2012.112
31 Domcke, S. *et al.* Competition between DNA methylation and transcription factors determines binding of NRF1. *Nature* **528**, 575-579 (2015). https://doi.org/10.1038/nature16462
32 Horvath, S. Erratum to: DNA methylation age of human tissues and cell types. *Genome Biol* **16**, 96 (2015). https://doi.org/10.1186/s13059-015-0649-6
33 Horvath, S. DNA methylation age of human tissues and cell types. *Genome Biol* **14**, R115 (2013). https://doi.org/10.1186/gb-2013-14-10-r115
34 Zhou, W. & Reizel, Y. On correlative and causal links of replicative epimutations. *Trends Genet* (2024). https://doi.org/10.1016/j.tig.2024.08.008
35 Duyckaerts, C. *et al.* PART is part of Alzheimer disease. *Acta Neuropathologica* **129**, 749-756 (2015). https://doi.org/10.1007/s00401-015-1390-7
36 Gourmaud, S. *et al.* Alzheimer-like amyloid and tau alterations associated with cognitive deficit in temporal lobe epilepsy. *Brain* **143**, 191-209 (2020). https://doi.org/10.1093/brain/awz381
37 Iida, M. A. *et al.* Predictors of cognitive impairment in primary age-related tauopathy: an autopsy study. *Acta Neuropathologica Communications* **9** (2021). https://doi.org/10.1186/s40478-021-01233-3
38 Josephs, K. A. *et al.* Tau aggregation influences cognition and hippocampal atrophy in the absence of beta-amyloid: a clinico-imaging-pathological study of primary age-related tauopathy (PART). *Acta Neuropathol* **133**, 705-715 (2017). https://doi.org/10.1007/s00401-017-1681-2
39 Teylan, M. *et al.* Cognitive trajectory in mild cognitive impairment due to primary age-related tauopathy. *Brain* **143**, 611-621 (2020). https://doi.org/10.1093/brain/awz403
40 Mesías, R. E. *et al.* Development and cadherin-mediated control of prefrontal corticostriatal projections in mice. *iScience* **26**, 108002 (2023). https://doi.org/10.1016/j.isci.2023.108002
41 Li, L. *et al.* Regulation of maternal behavior and offspring growth by paternally expressed Peg3. *Science* **284**, 330-333 (1999). https://doi.org/10.1126/science.284.5412.330
42 Fukushi, D. *et al.* <scp>R3HDM1</scp> haploinsufficiency is associated with mild intellectual disability. *American Journal of Medical Genetics Part A* **185**, 1776-1786 (2021). https://doi.org/10.1002/ajmg.a.62173

43 Cotney, J. *et al.* The autism-associated chromatin modifier CHD8 regulates other autism risk genes during human neurodevelopment. *Nature Communications* **6**, 6404 (2015). https://doi.org/10.1038/ncomms7404
44 Mulder, R. H. *et al.* Epigenome-wide change and variation in DNA methylation in childhood: trajectories from birth to late adolescence. *Hum Mol Genet* **30**, 119-134 (2021). https://doi.org/10.1093/hmg/ddaa280
45 Megraw, M. *et al.* Isoform specific gene auto-regulation via miRNAs: a case study on miR-128b and ARPP-21. *Theoretical Chemistry Accounts* **125**, 593-598 (2010). https://doi.org/10.1007/s00214-009-0647-4
46 Ching, A.-S. & Ahmad-Annuar, A. A Perspective on the Role of microRNA-128 Regulation in Mental and Behavioral Disorders. *Frontiers in Cellular Neuroscience* **9** (2015). https://doi.org/10.3389/fncel.2015.00465
47 Marangi, G., Orteschi, D., Milano, V., Mancano, G. & Zollino, M. Interstitial deletion of 3p22.3p22.2 encompassing ARPP21 and CLASP2 is a potential pathogenic factor for a syndromic form of intellectual disability: A co-morbidity model with additional copy number variations in a large family. *American Journal of Medical Genetics Part A* **161**, 2890-2893 (2013). https://doi.org/10.1002/ajmg.a.36257
48 Tan, C. L. *et al.* MicroRNA-128 Governs Neuronal Excitability and Motor Behavior in Mice. *Science* **342**, 1254-1258 (2013). https://doi.org/10.1126/science.1244193
49 Meftah, S. & Gan, J. Alzheimer's disease as a synaptopathy: Evidence for dysfunction of synapses during disease progression. *Frontiers in Synaptic Neuroscience* **15** (2023). https://doi.org/10.3389/fnsyn.2023.1129036
50 Tzioras, M., Mcgeachan, R. I., Durrant, C. S. & Spires-Jones, T. L. Synaptic degeneration in Alzheimer disease. *Nature Reviews Neurology* **19**, 19-38 (2023). https://doi.org/10.1038/s41582-022-00749-z
51 Morrison, J. H. & Baxter, M. G. The ageing cortical synapse: hallmarks and implications for cognitive decline. *Nature Reviews Neuroscience* **13**, 240-250 (2012). https://doi.org/10.1038/nrn3200
52 Petralia, R. S., Mattson, M. P. & Yao, P. J. Communication breakdown: The impact of ageing on synapse structure. *Ageing Research Reviews* **14**, 31-42 (2014). https://doi.org/10.1016/j.arr.2014.01.003
53 Frohlich, A. S. *et al.* Single-nucleus transcriptomic profiling of human orbitofrontal cortex reveals convergent effects of aging and psychiatric disease. *Nat Neurosci* **27**, 2021-2032 (2024). https://doi.org/10.1038/s41593-024-01742-z
54 Ling, E. *et al.* A concerted neuron-astrocyte program declines in ageing and schizophrenia. *Nature* **627**, 604-611 (2024). https://doi.org/10.1038/s41586-024-07109-5
55 Huijbers, W. *et al.* Tau Accumulation in Clinically Normal Older Adults Is Associated with Hippocampal Hyperactivity. *The Journal of Neuroscience* **39**, 548-556 (2019). https://doi.org/10.1523/jneurosci.1397-18.2018
56 Nguyen, T. A., Lehr, A. W. & Roche, K. W. Neuroligins and Neurodevelopmental Disorders: X-Linked Genetics. *Frontiers in Synaptic Neuroscience* **12** (2020). https://doi.org/10.3389/fnsyn.2020.00033
57 Ichtchenko, K., Nguyen, T. & Südhof, T. C. Structures, Alternative Splicing, and Neurexin Binding of Multiple Neuroligins. *Journal of Biological Chemistry* **271**, 2676-2682 (1996). https://doi.org/10.1074/jbc.271.5.2676
58 Yan, J. *et al.* Analysis of the neuroligin 4Y gene in patients with autism. *Psychiatric genetics.* **18**, 204-207 (2008). https://doi.org/10.1097/YPG.0b013e3282fb7fe6
59 Du, W. *et al.* Kinesin 1 Drives Autolysosome Tubulation. *Developmental Cell* **37**, 326-336 (2016). https://doi.org/https://doi.org/10.1016/j.devcel.2016.04.014
60 Correia, S. C., Perry, G. & Moreira, P. I. Mitochondrial traffic jams in Alzheimer's disease - pinpointing the roadblocks. *Biochimica et Biophysica Acta (BBA) - Molecular Basis of Disease* **1862**, 1909-1917 (2016). https://doi.org/https://doi.org/10.1016/j.bbadis.2016.07.010
61 Selvarasu, K. *et al.* Reduction of kinesin I heavy chain decreases tau hyperphosphorylation, aggregation, and memory impairment in Alzheimer's disease and tauopathy models. *Front Mol Biosci* **9**, 1050768 (2022). https://doi.org/10.3389/fmolb.2022.1050768

62 Williams, J. B., Cao, Q. & Yan, Z. Transcriptomic analysis of human brains with Alzheimer's disease reveals the altered expression of synaptic genes linked to cognitive deficits. *Brain Communications* **3** (2021). https://doi.org/10.1093/braincomms/fcab123
63 Li, H. *et al.* Identification of the molecular subgroups in Alzheimer's disease by transcriptomic data. *Frontiers in Neurology* **13** (2022). https://doi.org/10.3389/fneur.2022.901179
64 Crist, A. M. *et al.* Transcriptomic analysis to identify genes associated with selective hippocampal vulnerability in Alzheimer's disease. *Nature Communications* **12** (2021). https://doi.org/10.1038/s41467-021-22399-3
65 Otero-Garcia, M. *et al.* Molecular signatures underlying neurofibrillary tangle susceptibility in Alzheimer's disease. *Neuron* **110**, 2929-2948.e2928 (2022). https://doi.org/10.1016/j.neuron.2022.06.021
66 Chen, W.-T. *et al.* Spatial Transcriptomics and In Situ Sequencing to Study Alzheimer's Disease. *Cell* **182**, 976-991.e919 (2020). https://doi.org/10.1016/j.cell.2020.06.038
67 Rexach, J. E. *et al.* Tau Pathology Drives Dementia Risk-Associated Gene Networks toward Chronic Inflammatory States and Immunosuppression. *Cell Reports* **33**, 108398 (2020). https://doi.org/10.1016/j.celrep.2020.108398
68 Sanchez-Rodriguez, L. M. *et al.* In-vivo neuronal dysfunction by Aβ and tau overlaps with brain-wide inflammatory mechanisms in Alzheimer's disease. *Frontiers in Aging Neuroscience* **16** (2024). https://doi.org/10.3389/fnagi.2024.1383163
69 Mathys, H. *et al.* Single-cell transcriptomic analysis of Alzheimer's disease. *Nature* **570**, 332-337 (2019). https://doi.org/10.1038/s41586-019-1195-2
70 Caldwell, A. B. *et al.* Transcriptomic profiling of sporadic Alzheimer's disease patients. *Molecular Brain* **15** (2022). https://doi.org/10.1186/s13041-022-00963-2
71 Folstein, M. F., Robins, L. N. & Helzer, J. E. The Mini-Mental State Examination. *Arch Gen Psychiatry* **40**, 812 (1983). https://doi.org/10.1001/archpsyc.1983.01790060110016
72 Morris, J. C. The Clinical Dementia Rating (CDR): current version and scoring rules. *Neurology* **43**, 2412-2414 (1993). https://doi.org/10.1212/wnl.43.11.2412-a
73 Mirra, S. S. *et al.* The Consortium to Establish a Registry for Alzheimer's Disease (CERAD). Part II. Standardization of the neuropathologic assessment of Alzheimer's disease. *Neurology* **41**, 479-486 (1991). https://doi.org/10.1212/wnl.41.4.479
74 Kovacs, G. G. *et al.* Aging-related tau astrogliopathy (ARTAG): harmonized evaluation strategy. *Acta Neuropathol* **131**, 87-102 (2016). https://doi.org/10.1007/s00401-015-1509-x
75 Bennett, D. A. & Launer, L. J. Longitudinal epidemiologic clinical-pathologic studies of aging and Alzheimer's disease. *Curr Alzheimer Res* **9**, 617-620 (2012). https://doi.org/10.2174/156720512801322645
76 Smith, R. G. *et al.* Elevated DNA methylation across a 48-kb region spanning the HOXA gene cluster is associated with Alzheimer's disease neuropathology. *Alzheimers Dement* **14**, 1580-1588 (2018). https://doi.org/10.1016/j.jalz.2018.01.017
77 Marx, G. A. *et al.* Histopathologic brain age estimation via multiple instance learning. *Acta Neuropathologica* **146**, 785-802 (2023). https://doi.org/10.1007/s00401-023-02636-3
78 Bennett, D. A. *et al.* Pathological changes in frontal cortex from biopsy to autopsy in Alzheimer's disease. *Neurobiology of Aging* **14**, 589-596 (1993). https://doi.org/https://doi.org/10.1016/0197-4580(93)90043-B
79 Zhou, W., Triche, T. J., Laird, P. W. & Shen, H. SeSAMe: reducing artifactual detection of DNA methylation by Infinium BeadChips in genomic deletions. *Nucleic Acids Research* (2018). https://doi.org/10.1093/nar/gky691
80 Luo, C. *et al.* Single-cell methylomes identify neuronal subtypes and regulatory elements in mammalian cortex. *Science* **357**, 600-604 (2017). https://doi.org/10.1126/science.aan3351
81 Lee, D. S. *et al.* Simultaneous profiling of 3D genome structure and DNA methylation in single human cells. *Nat Methods* **16**, 999-1006 (2019). https://doi.org/10.1038/s41592-019-0547-z
82 Luo, C. *et al.* Single nucleus multi-omics identifies human cortical cell regulatory genome diversity. *Cell Genom* **2** (2022). https://doi.org/10.1016/j.xgen.2022.100107

83 Wang, Y., Grant, O. A., Zhai, X., McDonald-Maier, K. D. & Schalkwyk, L. C. Insights into ageing rates comparison across tissues from recalibrating cerebellum DNA methylation clock. *Geroscience* **46**, 39-56 (2024). https://doi.org/10.1007/s11357-023-00871-w
84 Kuhn, M. Building Predictive Models in R Using the caret Package. *Journal of Statistical Software* **28**, 1 - 26 (2008). https://doi.org/10.18637/jss.v028.i05
85 Chen, E. Y. *et al.* Enrichr: interactive and collaborative HTML5 gene list enrichment analysis tool. *BMC Bioinformatics* **14**, 128 (2013). https://doi.org/10.1186/1471-2105-14-128
86 Kuleshov, M. V. *et al.* Enrichr: a comprehensive gene set enrichment analysis web server 2016 update. *Nucleic Acids Res* **44**, W90-97 (2016). https://doi.org/10.1093/nar/gkw377
87 Xie, Z. *et al.* Gene Set Knowledge Discovery with Enrichr. *Curr Protoc* **1**, e90 (2021). https://doi.org/10.1002/cpz1.90

Appendix

The PART working group: Jean-Paul Vonsattel (Department of Pathology and Cell Biology, Department of Neurology, and the Taub Institute for Research on Alzheimer's Disease and the Aging Brain, Columbia University Medical Center, New York, NY), Andy F. Teich (Department of Pathology and Cell Biology, Department of Neurology, and the Taub Institute for Research on Alzheimer's Disease and the Aging Brain, Columbia University Medical Center, New York, NY), Marla Gearing (Department of Pathology and Laboratory Medicine (Neuropathology) and Neurology, Emory University School of Medicine, Atlanta, GA), Jonathan Glass (Department of Pathology and Laboratory Medicine (Neuropathology) and Neurology, Emory University School of Medicine, Atlanta, GA), Juan C. Troncoso (Department of Pathology, Division of Neuropathology, Johns Hopkins University School of Medicine, Baltimore, MD), Matthew P. Frosch (Department of Neurology and Pathology, Harvard Medical School and Massachusetts General Hospital, Charlestown, MA), Bradley T. Hyman (Department of Neurology and Pathology, Harvard Medical School and Massachusetts General Hospital, Charlestown, MA), Melissa E. Murray (Department of Neuroscience, Mayo Clinic, Jacksonville, FL), Johannes Attems (Translational and Clinical Research Institute, Newcastle University, Newcastle upon Tyne, UK), Margaret E. Flanagan (Department of Pathology (Neuropathology), Northwestern Cognitive Neurology and Alzheimer Disease Center, Northwestern University Feinberg School of Medicine, Chicago, IL), Qinwen Mao (Department of Pathology (Neuropathology), Northwestern Cognitive Neurology and Alzheimer Disease Center, Northwestern University Feinberg School of Medicine, Chicago, IL), M-Marsel Mesulam (Department of Pathology (Neuropathology), Northwestern Cognitive Neurology and Alzheimer Disease Center, Northwestern University Feinberg School of Medicine, Chicago, IL), Sandra Weintraub (Department of Pathology (Neuropathology), Northwestern Cognitive Neurology and Alzheimer Disease Center, Northwestern University Feinberg School of Medicine, Chicago, IL), Randy L. Woltjer (Department of Pathology, Oregon Health Sciences University, Portland, OR), Thao Pham (Department of Pathology, Oregon Health Sciences University, Portland, OR), Julia Kofler (Department of Pathology [Neuropathology], University of Pittsburgh Medical Center, Pittsburgh, PA), Julie A. Schneider (Departments of Pathology [Neuropathology] and Neurological Sciences, Rush University Medical Center, Chicago, IL), Lei Yu (Departments of Pathology [Neuropathology] and Neurological Sciences, Rush University Medical Center, Chicago, IL), Dushyant P. Purohit (Department of Pathology, Neuropathology Brain Bank and Research CoRE, Icahn School of Medicine at Mount Sinai, James J. Peters VA Medical Center, New York, NY), Vahram Haroutunian (Department of Psychiatry, Alzheimer's Disease Research Center, James J. Peters VA Medical Center, Nash Department of Neuroscience, Ronald M. Loeb Center for Alzheimer's Disease, Friedman Brain Institute, Icahn School of Medicine at Mount Sinai, New York, NY), Patrick R. Hof (Nash Department of Neuroscience, Ronald M. Loeb Center for Alzheimer's Disease, Friedman Brain Institute, Icahn School of Medicine at Mount Sinai, New York, NY), Sam Gandy (Departments of Psychiatry and Neurology, Center for Cognitive Health, Alzheimer's Disease Research Center, James J. Peters VA Medical Center, Icahn School of Medicine at Mount Sinai, New York, NY and Department of Icahn School of Medicine at Mount Sinai, New York, NY), Mary Sano (Department of Psychiatry, Alzheimer's Disease Research Center, James J. Peters VA Medical Center, Icahn School of Medicine at Mount Sinai, New York, NY), Thomas G. Beach (Department of Neuropathology, Banner Sun Health Research Institute, Sun City, AZ), Wayne Poon (Department of Neurology, Department of Epidemiology, Institute for Memory Impairments and Neurological Disorders, UC Irvine, Irvine, CA), Claudia H. Kawas (Department of Neurology, Department of Neurobiology and Behavior, Institute for Memory Impairments and Neurological Disorders, UC Irvine, Irvine, CA), María M. Corrada (Department of Neurology, Department of Epidemiology, Institute for Memory Impairments and Neurological Disorders, UC Irvine, Irvine, CA), Robert A. Rissman (Department of Neurosciences University of California and the Veterans Affairs San Diego Healthcare System, La Jolla, San Diego, CA), Jeff Metcalf (Department of Neurosciences University of California and the Veterans Affairs San Diego Healthcare System, La Jolla, San Diego, CA), Sara Shuldberg (Department of Neurosciences University of California and the Veterans Affairs San Diego Healthcare System, La Jolla, San Diego, CA), Bahar Salehi (Department of Neurosciences University of California and the Veterans Affairs San Diego Healthcare System, La Jolla, San Diego, CA), Peter T. Nelson (Department of Pathology [Neuropathology] and Sanders-Brown Center on Aging, University of Kentucky, Lexington, KY), John Q. Trojanowski (Center for Neurodegenerative Disease Research, Department of Pathology and Laboratory Medicine, Perelman School of Medicine, University of Pennsylvania, Philadelphia,

PA), Edward B. Lee (Center for Neurodegenerative Disease Research, Department of Pathology and Laboratory Medicine, Perelman School of Medicine, University of Pennsylvania, Philadelphia, PA), David A. Wolk (Department of Neurology, Perelman School of Medicine, University of Pennsylvania, Philadelphia, PA), Corey T. McMillan (Department of Neurology, Perelman School of Medicine, University of Pennsylvania, Philadelphia, PA), C. Dirk Keene (Department of Laboratory Medicine and Pathology, University of Medicine, Seattle, WA), Caitlin S. Latimer (Department of Laboratory Medicine and Pathology, University of Medicine, Seattle, WA), Thomas J. Montine (Department of Laboratory Medicine and Pathology, University of Medicine, Seattle, WA and Department of Pathology, Stanford University, Palo Alto, CA), Gabor G. Kovacs (Laboratory Medicine Program, Krembil Brain Institute, University Health Network, Toronto, ON, Canada, Tanz Centre for Research in Neurodegenerative Disease and Department of Laboratory Medicine and Pathobiology, University of Toronto, Toronto, Ontario, Canada, and Institute of Neurology, Medical University of Vienna, Vienna, Austria), Mirjam I. Lutz (Institute of Neurology, Medical University of Vienna, Vienna, Austria), Peter Fischer (Department of Psychiatry, Danube Hospital, Vienna, Austria), Richard J Perrin (Department of Pathology and Immunology, Department of Neurology, Knight Alzheimer Disease Research Center, Washington University School of Medicine, St. Louis, MO), Nigel J. Cairns (College of Medicine and Health, University of Exeter, Exeter, UK).

Fig. 1

a

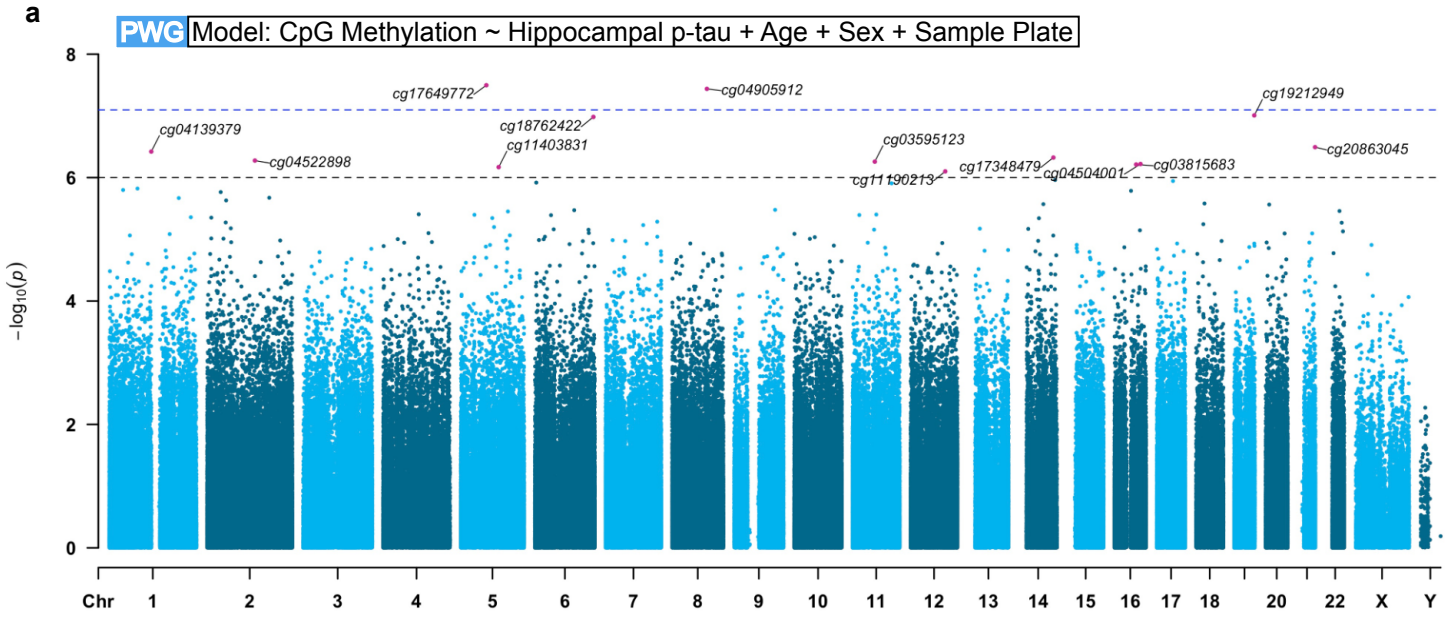

b

PWG EWAS (n=176)				ROSMAP (n=513)					
CpG	CpG ~ log(p-Tau) Effect Size	FDR	CpG Proximal Gene (10KB)	Methylation-Proximal Gene Exp Correlation (ROSMAP)	P	FDR	Gene ~ log(p-Tau) Effect Size	P	FDR
cg17649772	-0.05721	0.0128	ANKRA2	CpG not on HM450			-0.21004	0.24795	0.35126
cg17649772	-0.05721	0.0128	UTP15				-0.28974	0.11380	0.21496
cg04905912	-0.10131	0.0128	No proximal gene within 10KB						
cg18762422	-0.19215	0.0183	RPS6KA2	0.02339	0.59714	0.96490	0.05347	0.82275	0.82275
cg18762422	-0.19215	0.0183	MIR1913	Expression data NA / 0					
cg19212949	-0.04472	0.0183	AC006115.2						
cg19212949	-0.04472	0.0183	ZIM2						
cg19212949	-0.04472	0.0183	PEG3	-0.11446	0.00947	0.037881628	-0.20881	0.07226	0.15695
cg03595123	-0.09459	0.0392	RTN3	0.09106	0.03924	0.09937	-0.17309	0.01637	0.05567
cg03815683	-0.05125	0.0392	CDH8	0.12926	0.00336	0.02016	-0.31494	0.00522	0.02959
cg04139379	-0.06454	0.0392	PHGDH	CpG not on HM450			0.11062	0.35335	0.46207
cg04504001	-0.05951	0.0392	AC138627.1	0.02003	0.65090	0.96490	-0.15488	0.72596	0.77133
cg04504001	-0.05951	0.0392	PSMD7	-0.00050	0.99104	0.99104	-0.31625	0.07342	0.15695
cg04504001	-0.05951	0.0392	AC009120.2	-0.00643	0.88449	0.96490	-0.09130	0.66052	0.74858
cg04504001	-0.05951	0.0392	AC009120.1	0.01713	0.69868	0.96490	0.22057	0.07386	0.15695
cg04504001	-0.05951	0.0392	AC009120.3	Expression data NA / 0					
cg04522898	-0.06836	0.0392	ZRANB3	0.09008	0.04140	0.09937	-0.79485	0.00042	0.00716
cg04522898	-0.06836	0.0392	R3HDM1	0.18551	0.00002	0.00028	-0.21534	0.00906	0.03850
cg17348479	-0.10813	0.0392	AL137786.1	0.00753	0.86491	0.96490	-0.44481	0.00123	0.01042
cg20863045	-0.11313	0.0392	PCBP3	CpG not on HM450			-0.09405	0.51425	0.62445
cg20863045	-0.11313	0.0392	AL133492.1	Expression data NA / 0					
cg11403831	-0.05541	0.0397	FER	-0.00964	0.82750	0.96490	0.47104	0.14856	0.25256
cg11190213	-0.05846	0.0429	LINC02453	CpG not on HM450			-0.42477	0.20586	0.31814

c

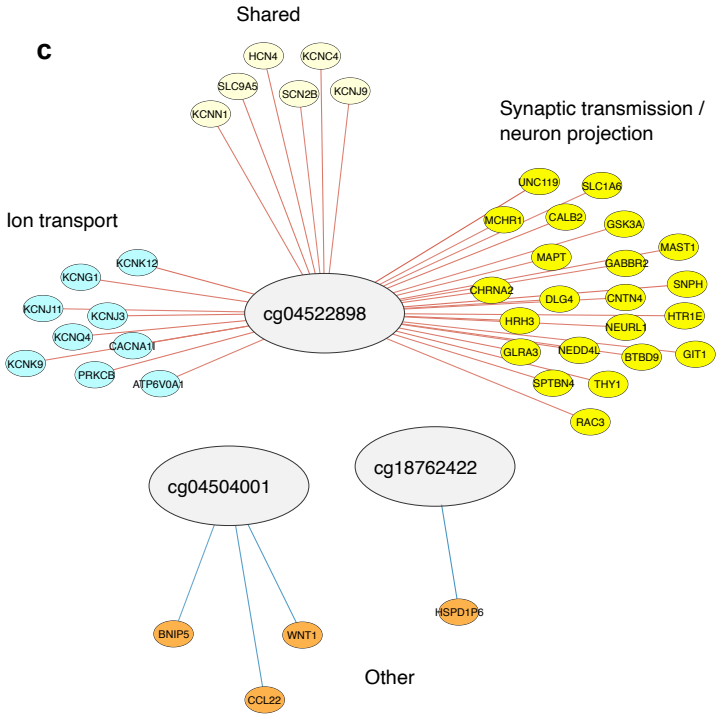

d

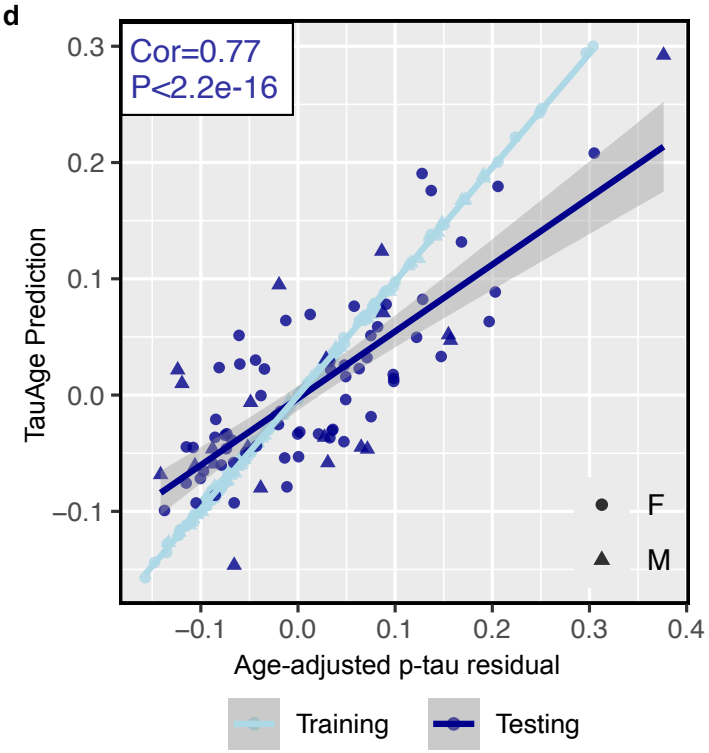

Fig. 2

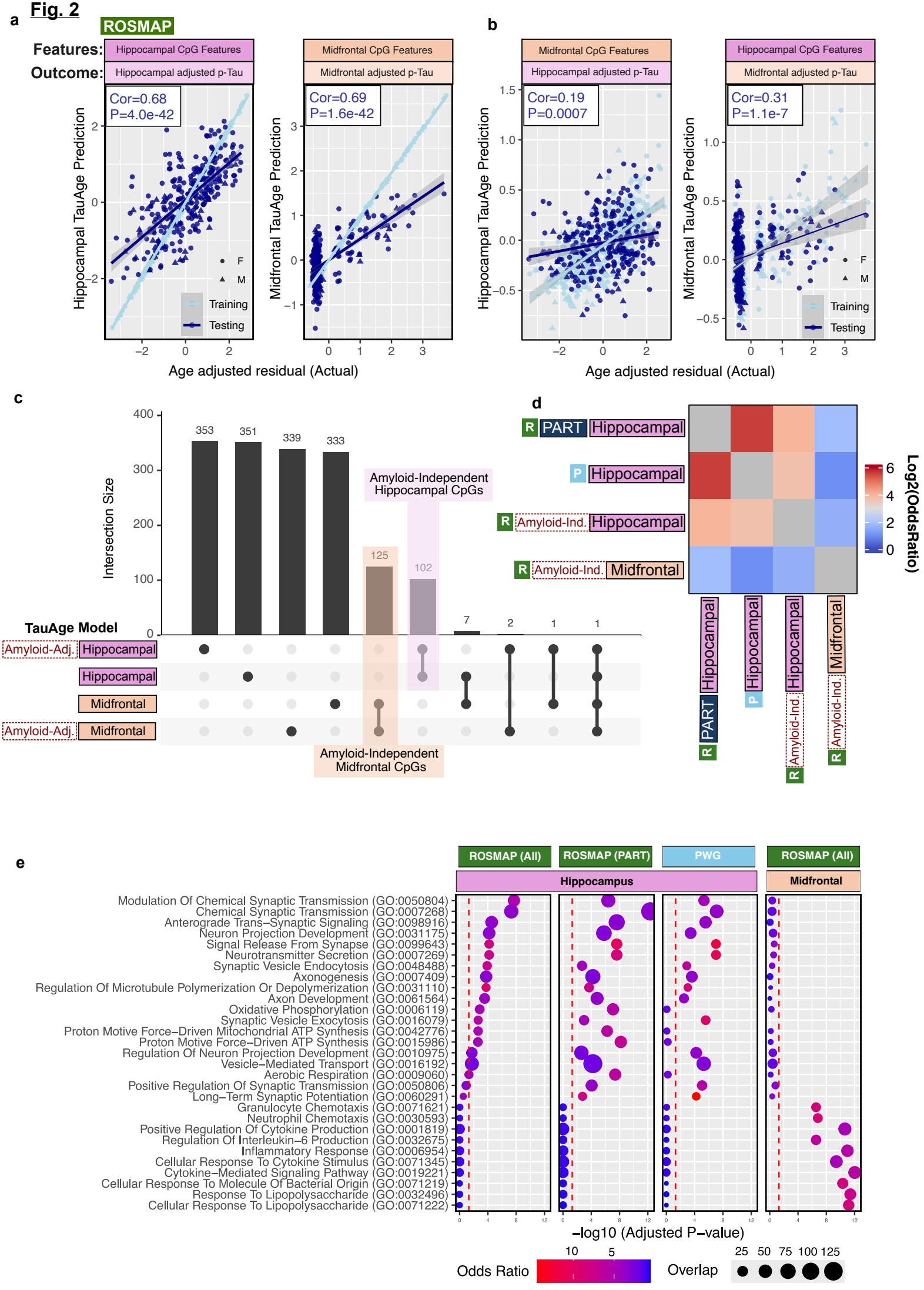
a
ROSMAP
Features:
Outcome:
Hippocampal CpG Features
Hippocampal adjusted p-Tau
Cor=0.68
P=4.0e-42
Hippocampal TauAge Prediction
Midfrontal CpG Features
Midfrontal adjusted p-Tau
Cor=0.69
P=1.6e-42
Midfrontal TauAge Prediction
F
M
Training
Testing
Age adjusted residual (Actual)
b
Cor=0.19
P=0.0007
Cor=0.31
P=1.1e-7
c
Intersection Size
353
351
339
333
125
102
7
2
1
1
Amyloid-Independent Hippocampal CpGs
Amyloid-Independent Midfrontal CpGs
TauAge Model
Amyloid-Adj. Hippocampal
Hippocampal
Midfrontal
Amyloid-Adj. Midfrontal
d
R PART Hippocampal
P Hippocampal
R Amyloid-Ind. Hippocampal
R Amyloid-Ind. Midfrontal
Log2(OddsRatio)
e
ROSMAP (All)
ROSMAP (PART)
PWG
ROSMAP (All)
Hippocampus
Midfrontal
Modulation Of Chemical Synaptic Transmission (GO:0050804)
Chemical Synaptic Transmission (GO:0007268)
Anterograde Trans−Synaptic Signaling (GO:0098916)
Neuron Projection Development (GO:0031175)
Signal Release From Synapse (GO:0099643)
Neurotransmitter Secretion (GO:0007269)
Synaptic Vesicle Endocytosis (GO:0048488)
Axonogenesis (GO:0007409)
Regulation Of Microtubule Polymerization Or Depolymerization (GO:0031110)
Axon Development (GO:0061564)
Oxidative Phosphorylation (GO:0006119)
Synaptic Vesicle Exocytosis (GO:0016079)
Proton Motive Force−Driven Mitochondrial ATP Synthesis (GO:0042776)
Proton Motive Force−Driven ATP Synthesis (GO:0015986)
Regulation Of Neuron Projection Development (GO:0010975)
Vesicle−Mediated Transport (GO:0016192)
Aerobic Respiration (GO:0009060)
Positive Regulation Of Synaptic Transmission (GO:0050806)
Long−Term Synaptic Potentiation (GO:0060291)
Granulocyte Chemotaxis (GO:0071621)
Neutrophil Chemotaxis (GO:0030593)
Positive Regulation Of Cytokine Production (GO:0001819)
Regulation Of Interleukin−6 Production (GO:0032675)
Inflammatory Response (GO:0006954)
Cellular Response To Cytokine Stimulus (GO:0071345)
Cytokine−Mediated Signaling Pathway (GO:0019221)
Cellular Response To Molecule Of Bacterial Origin (GO:0071219)
Response To Lipopolysaccharide (GO:0032496)
Cellular Response To Lipopolysaccharide (GO:0071222)
−log10 (Adjusted P−value)
Odds Ratio
Overlap

Fig. 3

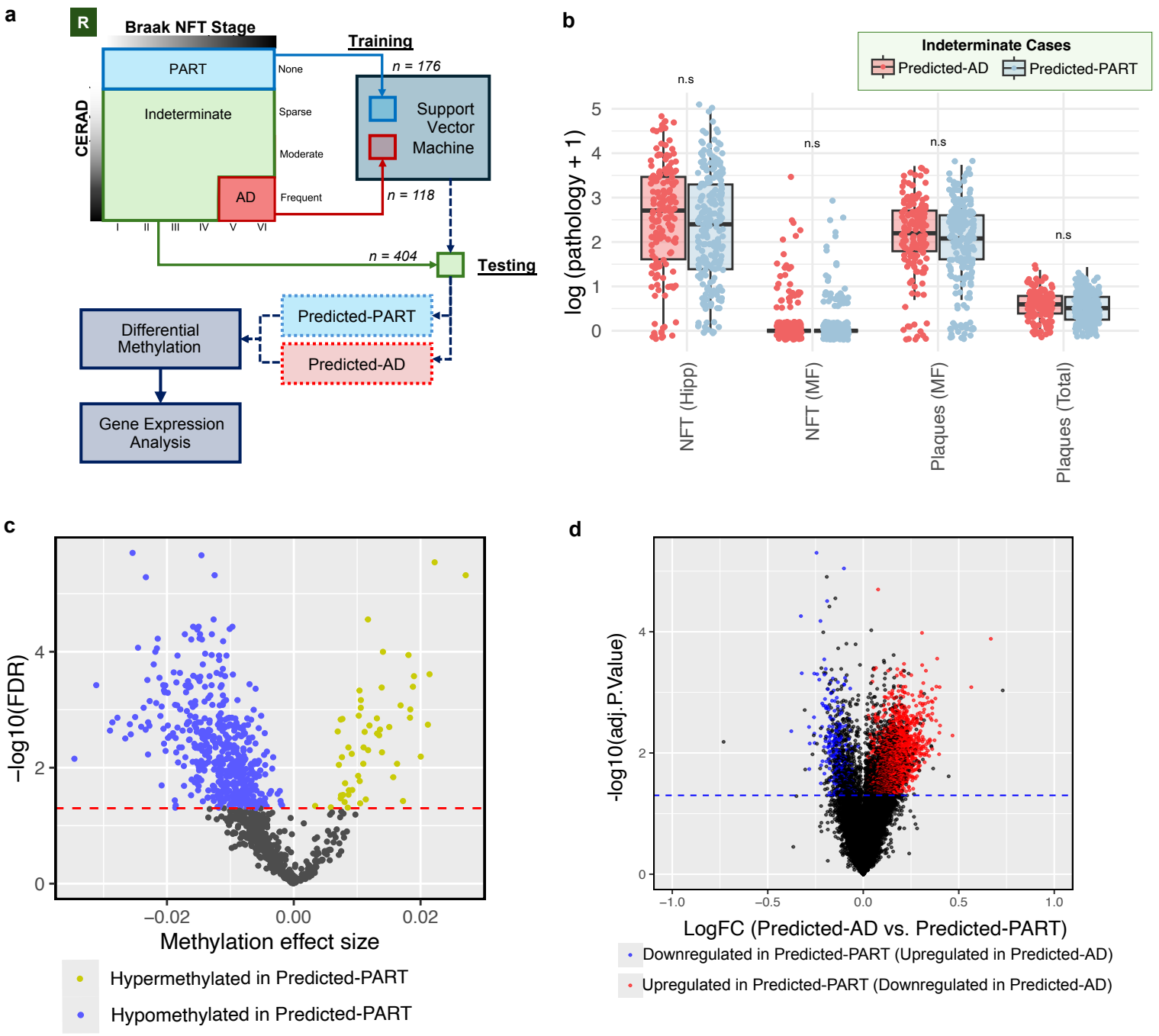
a
R
Braak NFT Stage
CERAD
PART
Indeterminate
AD
None
Sparse
Moderate
Frequent
I
II
III
IV
V
VI
Training
n = 176
Support Vector Machine
n = 118
n = 404
Testing
Predicted-PART
Predicted-AD
Differential Methylation
Gene Expression Analysis
b
Indeterminate Cases
Predicted-AD
Predicted-PART
log (pathology + 1)
n.s
NFT (Hipp)
NFT (MF)
Plaques (MF)
Plaques (Total)
c
−log10(FDR)
Methylation effect size
Hypermethylated in Predicted-PART
Hypomethylated in Predicted-PART
d
-log10(adj.P.Value)
LogFC (Predicted-AD vs. Predicted-PART)
Downregulated in Predicted-PART (Upregulated in Predicted-AD)
Upregulated in Predicted-PART (Downregulated in Predicted-AD)

Fig. 4

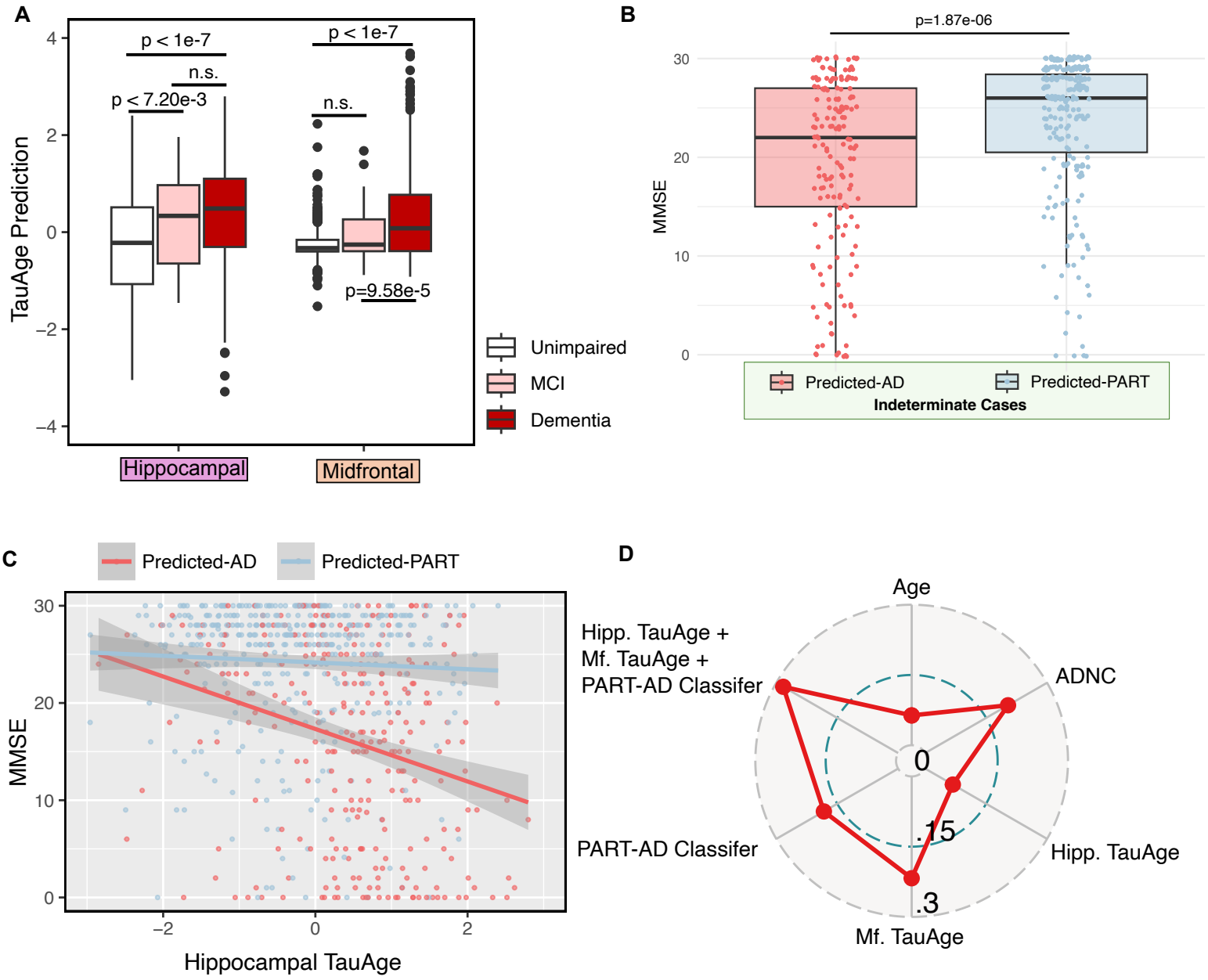
A
TauAge Prediction
p < 1e-7
n.s.
p < 7.20e-3
p < 1e-7
n.s.
p=9.58e-5
Hippocampal
Midfrontal
Unimpaired
MCI
Dementia
B
p=1.87e-06
MMSE
Predicted-AD
Predicted-PART
Indeterminate Cases
C
Predicted-AD
Predicted-PART
MMSE
Hippocampal TauAge
D
Age
ADNC
Hipp. TauAge
Mf. TauAge
PART-AD Classifer
Hipp. TauAge +
Mf. TauAge +
PART-AD Classifer
0
.15
.3

Extended Data Fig. 1

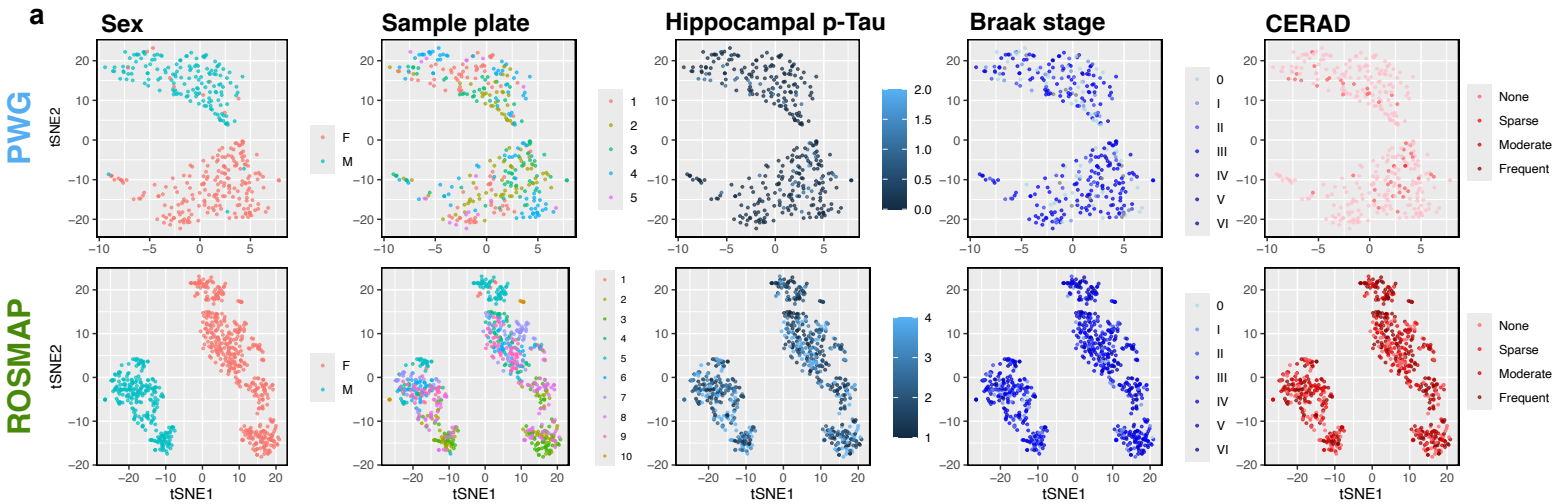

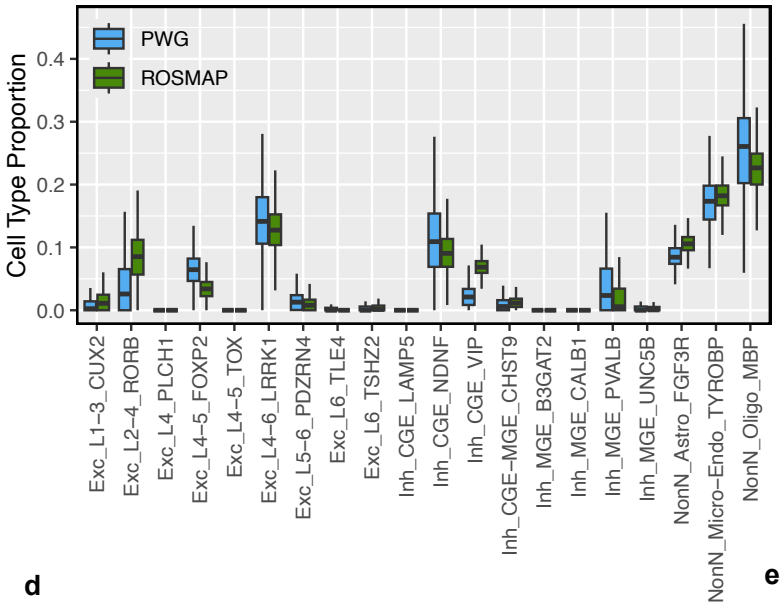

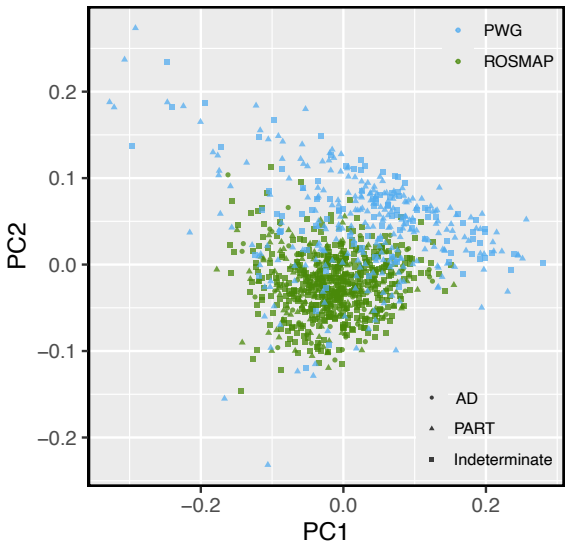

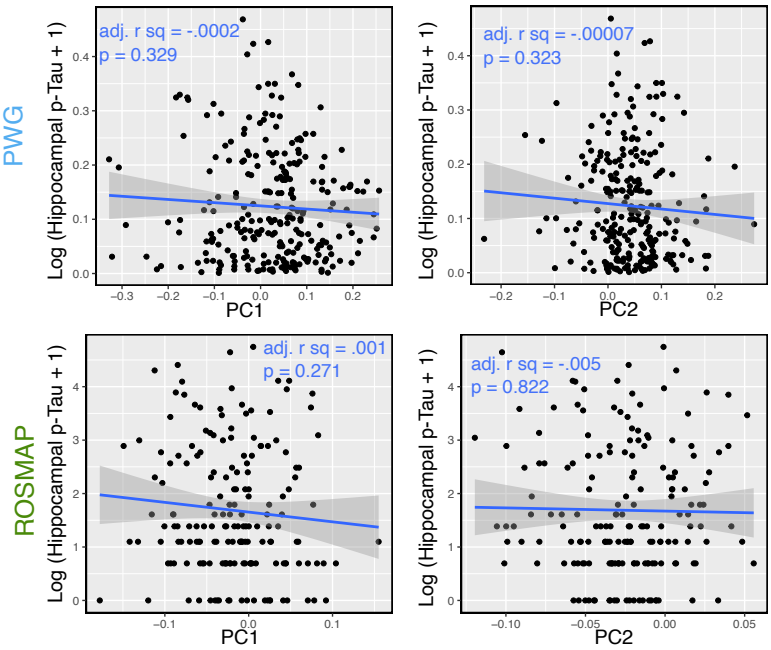

e

Model: Log (Hippocampal p-tau + 1) ~ Age + Sex + Cell Type Proportion			
CellType	Cell Type Coefficients		
	estimate	P	FDR
Exc_L1_3_CUX2	1.0818	0.02171	0.40589
Exc_L2_4_RORB	0.1630	0.18084	0.60279
Exc_L4_5_FOXP2	0.1240	0.57558	0.97032
Exc_L4_5_TOX	0.8250	0.63714	0.97032
Exc_L4_6_LRRK1	0.0179	0.87329	0.97032
Exc_L4_PLCH1	-1.3193	0.75646	0.97032
Exc_L5_6_PDZRN4	0.5294	0.14456	0.57822
Exc_L6_TLE4	0.2510	0.81081	0.97032
Exc_L6_TSHZ2	0.1982	0.82872	0.97032
Inh_CGE_LAMP5	-0.9975	0.45480	0.97032
Inh_CGE_MGE_CHST9	0.3834	0.47491	0.97032
Inh_CGE_NDNF	-0.0418	0.65974	0.97032
Inh_CGE_VIP	0.5493	0.08118	0.40589
Inh_MGE_B3GAT2	-1.4588	0.04519	0.40589
Inh_MGE_CALB1	-0.0065	0.97498	0.97805
Inh_MGE_PVALB	-0.0408	0.76213	0.97032
Inh_MGE_UNC5B	0.9846	0.22967	0.65621
NonN_Astro_FGF3R	0.1373	0.56920	0.97032
NonN_Micro_Endo_TYROBP	-0.0033	0.97805	0.97805
NonN_Oligo_MBP	-0.1277	0.07607	0.40589

Extended Data Fig. 2

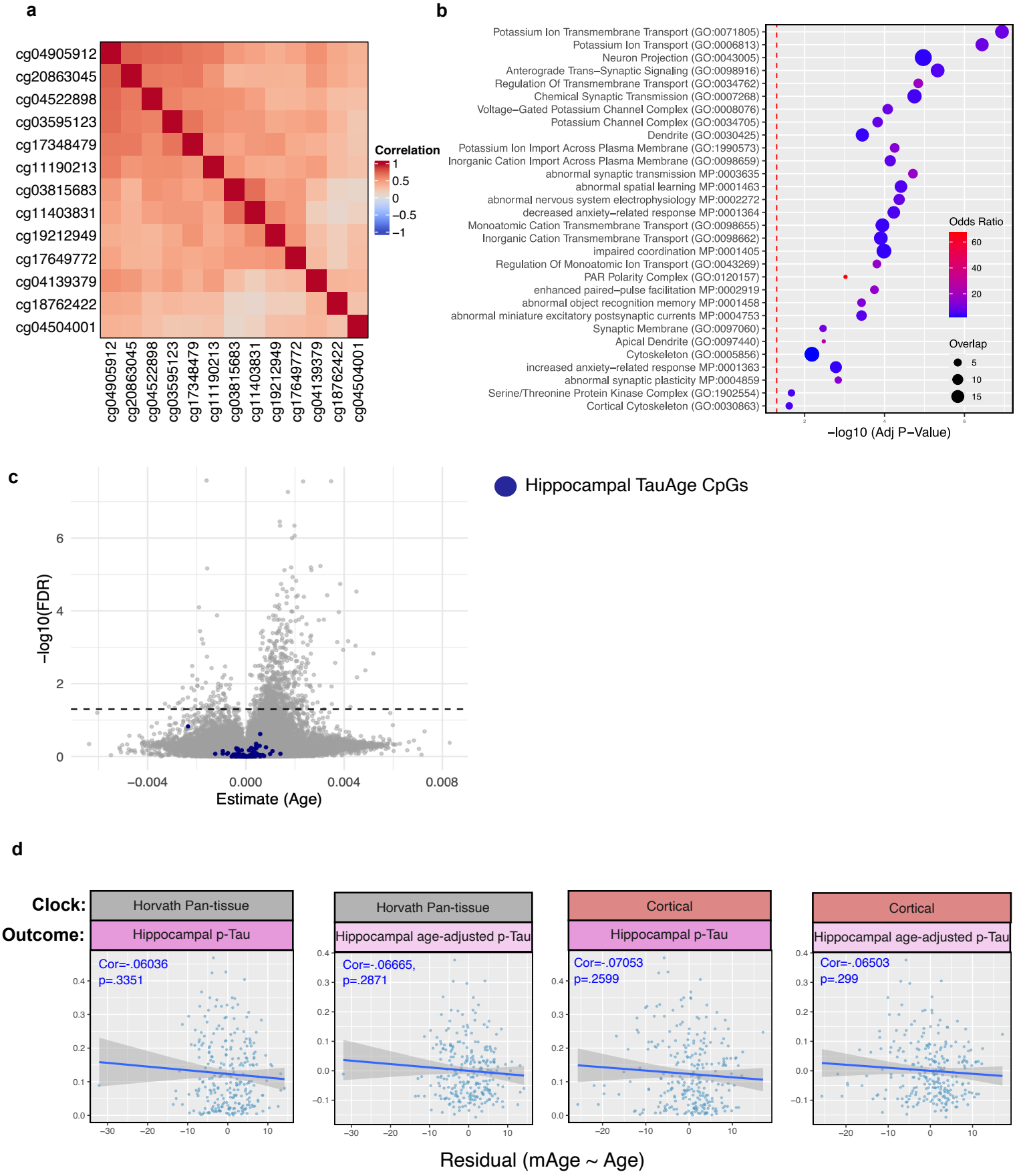

Extended Data Fig. 3

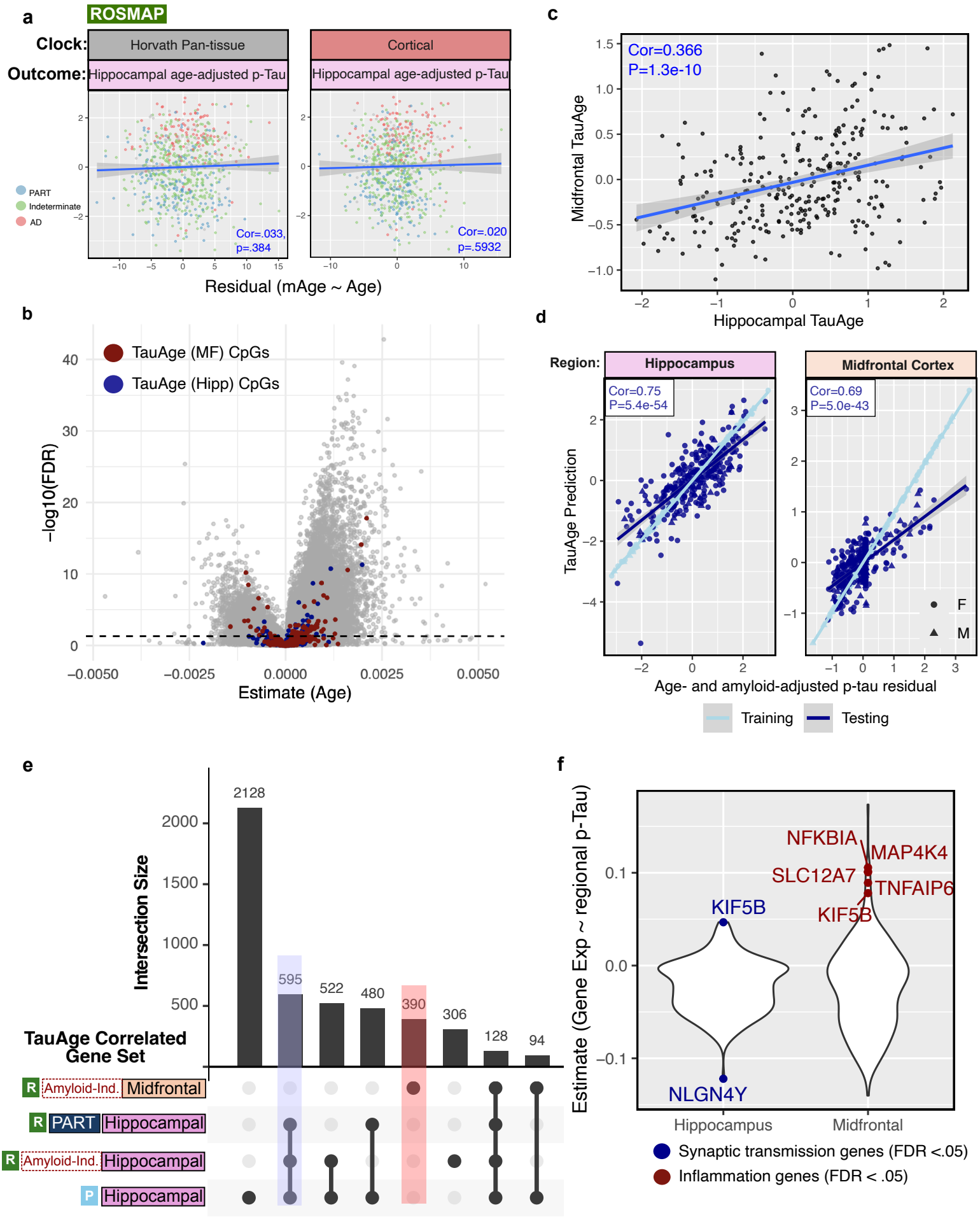

Extended Data Fig. 4

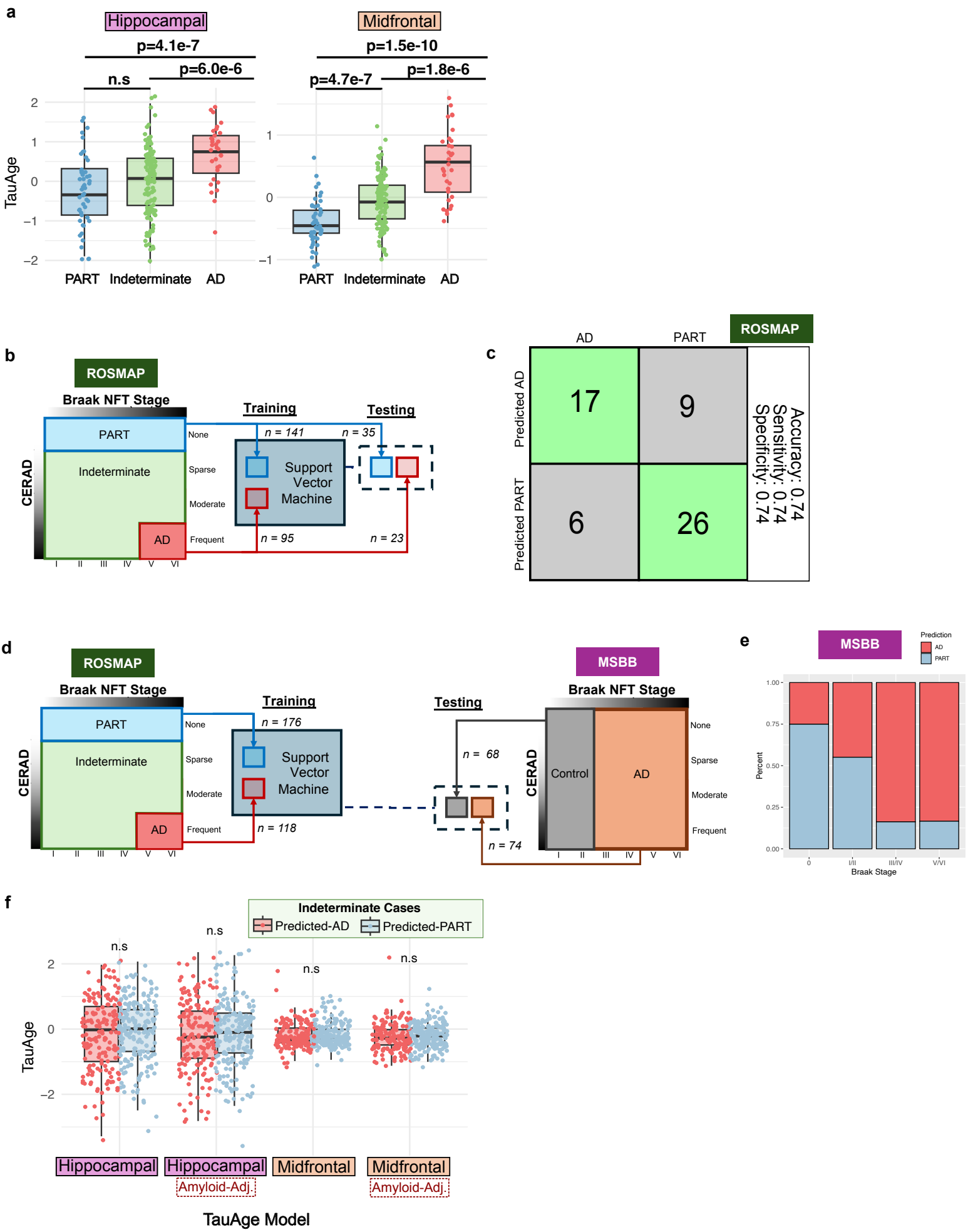

Extended Data Fig. 5

a

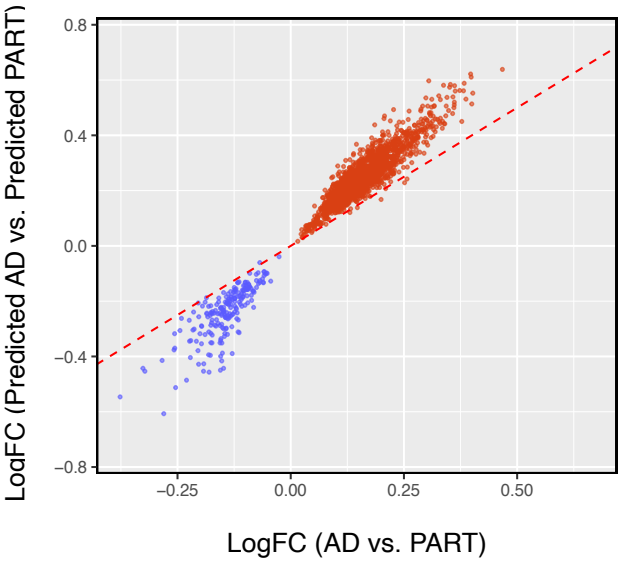

c

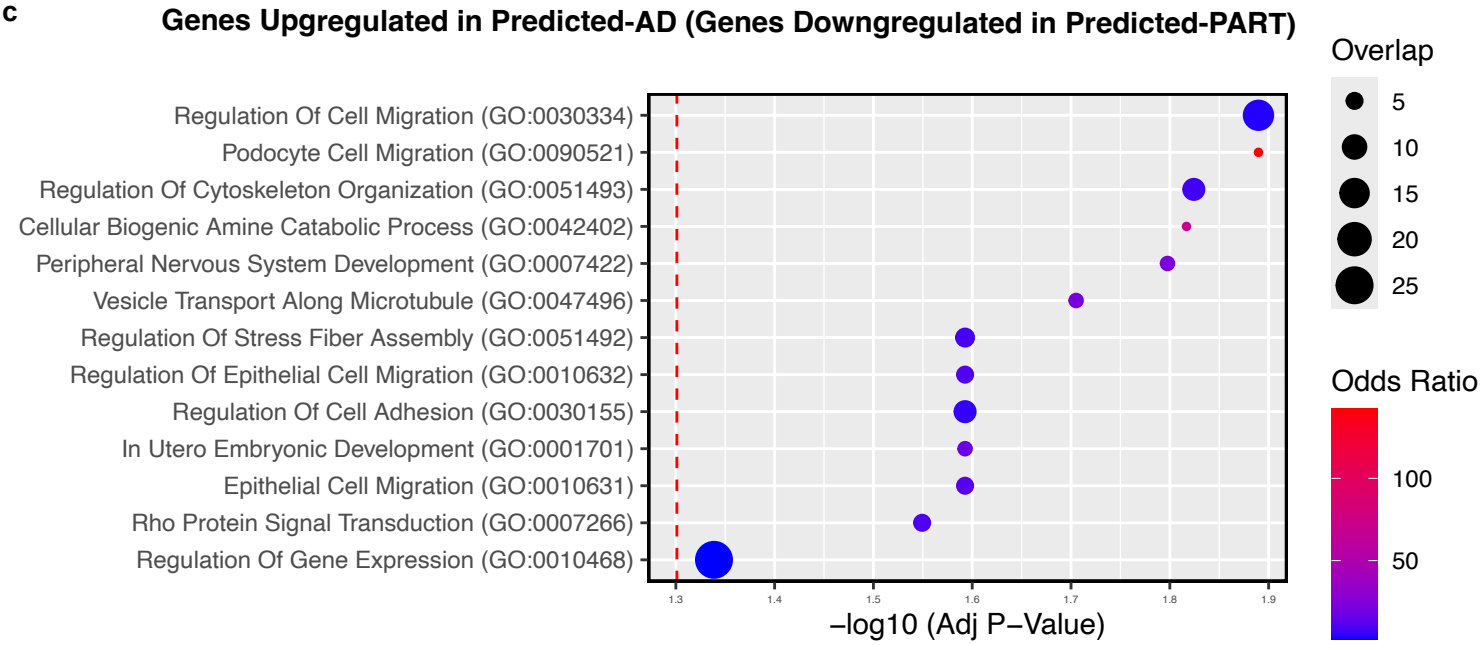
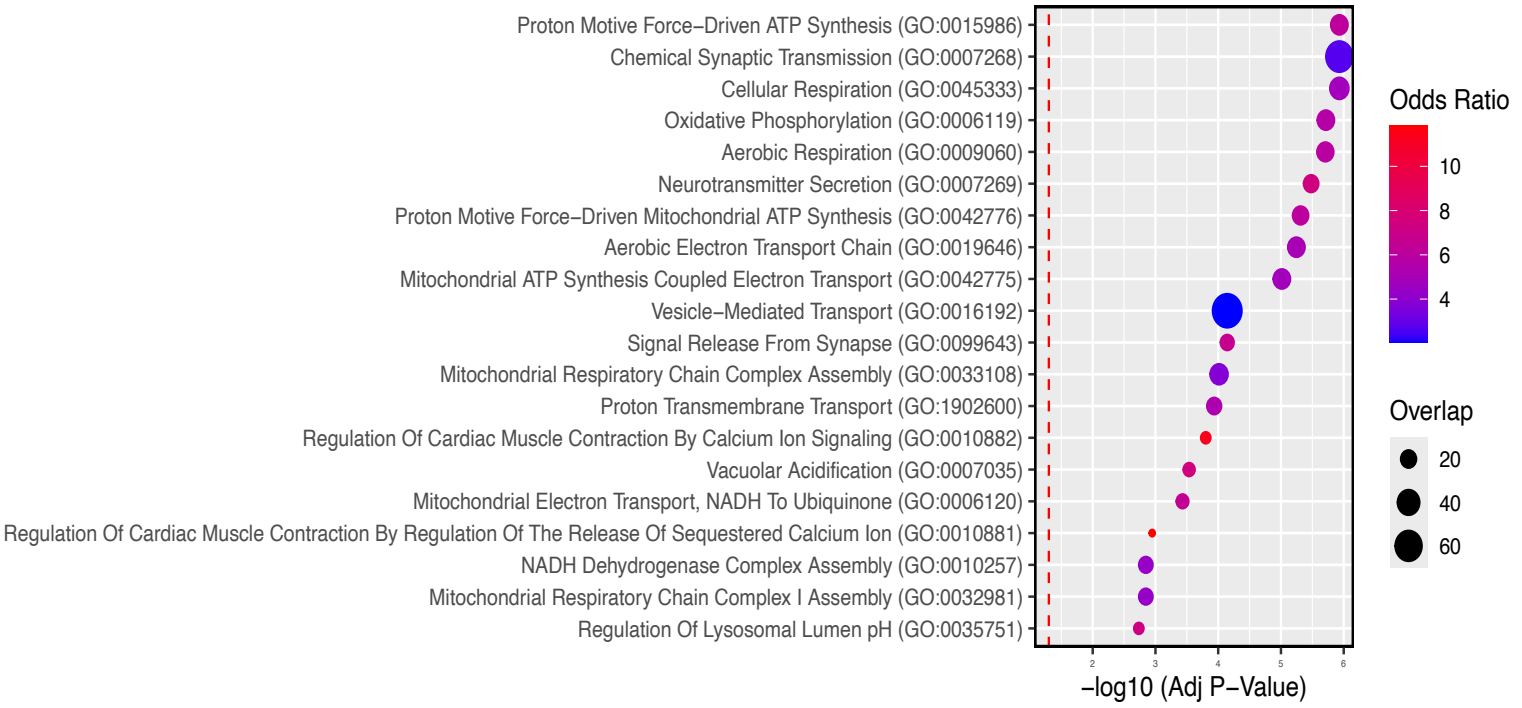
d